RRA-T7905
1 APRIL 1979

RRA RADIATION RESEARCH ASSOCIATES
Fort Worth, Texas

TIME DELAY AND PULSE STRETCHING CALCULATIONS FOR LASER RADIATION PROPAGATION IN CLOUDS

D. G. COLLINS

INTERIM REPORT
PREPARED UNDER
CONTRACT NO. 13-1370

APPROVED FOR PUBLIC RELEASE: DISTRIBUTION IS UNLIMITED

PREPARED FOR

SANDIA LABORATORIES
ALBUQUERQUE, NEW MEXICO 87185

UNCLASSIFIED

SECURITY CLASSIFICATION OF THIS PAGE (When Data Entered)

REPORT DOCUMENTATION PAGE		READ INSTRUCTIONS BEFORE COMPLETING FORM
1. REPORT NUMBER RRA-T7905	2. GOVT ACCESSION NO.	3. RECIPIENT'S CATALOG NUMBER
4. TITLE (and Subtitle) TIME DELAY AND PULSE STRETCHING CALCULATIONS FOR LASER RADIATION PROPAGATION IN CLOUDS		5. TYPE OF REPORT & PERIOD COVERED Interim 6. PERFORMING ORG. REPORT NUMBER RRA-T7905
7. AUTHOR(s) DAVE G. COLLINS		8. CONTRACT OR GRANT NUMBER(s) 13-1370
9. PERFORMING ORGANIZATION NAME AND ADDRESS RADIATION RESEARCH ASSOCIATES, INC. 3550 Hulen Street Fort Worth, Texas 76107		10. PROGRAM ELEMENT, PROJECT, TASK AREA & WORK UNIT NUMBERS
11. CONTROLLING OFFICE NAME AND ADDRESS Sandia Laboratories Albuquerque, NM 87185		12. REPORT DATE 1 April 1979 13. NUMBER OF PAGES 56
14. MONITORING AGENCY NAME & ADDRESS(if different from Controlling Office)		15. SECURITY CLASS. (of this report) Unclassified 15a. DECLASSIFICATION/DOWNGRADING SCHEDULE

16. DISTRIBUTION STATEMENT (of this Report)

APPROVED FOR PUBLIC RELEASE: DISTRIBUTION IS UNLIMITED
per Sandia Monitor 4/15/94

17. DISTRIBUTION STATEMENT (of the abstract entered in Block 20, if different from Report)

18. SUPPLEMENTARY NOTES

19. KEY WORDS (Continue on reverse side if necessary and identify by block number)

Light Scattering
Pulse Stretching
Clouds
Mie Scattering

20. ABSTRACT (Continue on reverse side if necessary and identify by block number)

A computer study was conducted to determine the effects of multiple scattering on the time delay and stretching of a laser pulse propagating within a cloudy atmosphere. An effort was made to model the experimental setup and cloud conditions that existed during Project CLIPS conducted by Sandia Laboratories on Hawaii Island in the Fall of 1978. The scattering and extinction coefficients and the angular scattering distributions were calculated for several cloud conditions using measured cloud aerosol size distributions furnished by

DD FORM 1473 EDITION OF 1 NOV 65 IS OBSOLETE

UNCLASSIFIED

SECURITY CLASSIFICATION OF THIS PAGE (When Data Entered)

Sandia Laboratories. Two sets of cloud conditions were chosen for use in modeling the time-dependent laser propagation studies. The optical distance between the laser source and telescope receiver separated by a distance of 765 meters was 5.3 for one cloud model and 14.7 for the other.

Calculations of the time delay and pulse stretching were made for the source and receiver elevated at various angles above the source-receiver axis. The maximum elevation considered for both the source and receiver was 10 degrees. The largest time delays and the maximum pulse stretching were calculated when both the source and receiver were elevated at 10 degrees from the source-receiver axis. The time delays calculated for the highly collimated source and receiver are predicted by the time delay of the single scattered radiation. This was true even when the single scattering was an insignificant portion of the total scattered radiation received during the time that single scattering is possible.

The maximum time delay calculated for the two cloud models with the source and receiver elevated 10 degrees above the source-receiver axis was approximately 40 nanoseconds. The maximum pulse stretching determined was an approximate 4 nanosecond increase in the pulse width at half maximum for an original pulse that was 10 nanoseconds in width at half-maximum.

TABLE OF CONTENTS

LIST OF FIGURES

LIST OF FIGURES (Continued)

LIST OF FIGURES (Continued)

LIST OF TABLES

I. INTRODUCTION

A continuing study is being conducted at Radiation Research Associates, Inc. to determine the effects of multiple scattering on the time delay and pulse stretching of laser pulses propagating within cloudy atmospheres (Refs. 1 and 2). The particular phase of the study to be discussed in this report involves an effort to model the atmospheric conditions and the experimental setup of Project CLIPS (Cloud-Induced Pulse Stretching) conducted by Sandia Laboratories during recent tests in the Hawaiian Islands. The TPART-III time dependant radiation transport Monte Carlo program is being utilized in the study (Ref. 3). The specific objective of the study was to note the effects upon the time delay and stretching of the scattered pulse observed when the laser beam and the receiver field-of-view were scanned off the source-receiver axis.

Modeling of the experimental setup is discussed in Section II. In addition, a description of the atmospheric models used in the calculation is presented in Section II.

The results of the calculations made for two different cloud conditions are presented in Section III.

II. MODELING OF EXPERIMENT

The TPART-III program was used to model the experimental set-up of the laser time delay and pulse-stretching measurements conducted by Sandia Laboratories during the Fall of 1978 in the saddle region on the island of Hawaii. The laser transmitter was modeled in TPART-III as a monochromatic source emitting a uniform intensity beam 2.5 inches in diameter at the source with the beam having a divergence of 0.1 milliradian. The TPART-III calculations were performed assuming instantaneous emission.

An auxiliary routine was used to convolve a Gaussian pulse 10 nanoseconds wide at half maximum with the time-dependent transmission data computed for an instantaneous emitting pulse.

The telescope receiver was modeled as an annular ring receiver with an inner radius of 2.25 inches and an outer radius of 7 inches. Each point on the annular receiver surface is assumed to have a conical field-of-view. Although responses to the cloud scattered radiation were calculated for receiver fields-of-view of 0.03, 0.1, 0.3 and 1.0 degrees, the statistical reliability of the response for an 1.0 degree field-of-view was much better than that for the smaller fields-of-view and, therefore, only that data for the 1.0 degree field-of-view were analyzed for this report.

All calculations were made for the transmitter operating in the visible at a wavelength of 532 nanometers and for the transmitter and receiver in what is nominally called the "scanning" configuration. In this configuration the transmitter and receiver were separated by a distance of 765 meters. Although the terrain beneath the beam was not smooth, it was modeled in the TPART-III calculations as a smooth Lambertian reflection surface 25 meters below the beam. This was estimated to be the average height of this beam above the ground surface between the transmitter and receiver. After a review of measured data for terrain albedoes in the Hawaiian Islands region and for the type of terrain existing at the test site, (Ref. 4) a ground albedo of 0.08 was selected to represent the albedo for ground reflections at the 532 nanometer wavelength.

The cloud extinction coefficients and angular scattering distributions used in the TPART-III calculations were determined from measurements of the cloud aerosol size distributions taken at the test site during the same times that the laser beam scanning measurements were being taken. Sandia Laboratories furnished the measurements of the cloud aerosol size distribution taken during a three-hour period on the date of 16 November 1978. Table I presents a summary of that data. The column labeled PROBE indicates which of the two Particle Measuring System (PMS) probes was the source of the data. With the PMS probe FSSP-100, aerosol particle size distributions covering the diameter range from 2 to 47 microns were measured. With the PMS probe OAP-200X, aerosol particle size distributions covering the diameter range from 20 to 300 microns were measured. Note that there is an overlap in the particle diameter ranges measured with the two different probes.

The cloud extinction coefficients that were computed for the size distributions measured with the two different probes are listed in Table II. The index of refraction for water at a wavelength of 532 nanometers, $1.335 - 1.3 * 10^{-9}i$, was used for the cloud aerosol particles in the MIE-II calculations run to compute the scattering and extinction coefficients (Ref. 5). The meteorological ranges listed in Table II were derived by dividing 3.912 by the extinction coefficient and converting the units from kilometers to meters. Calculations were also made for aerosol size distributions which resulted from combining the cloud particle size distributions measured with the two different probes. The cloud particle size distribution measured by the two different probes at 14:09 and 14:15 and at 14:37 and 14:51 were combined to provide two different size distributions that described cloud particles ranging from 2 to 160 microns in diameter. Although the OAP-200X probe was capable of measuring particle diameter ranges to 320 microns, the measured data showed no significant amounts of cloud aerosols in the diameter intervals above 160 microns. Two different methods were used in combining the size distributions measured with the OAP-200X and the FSSP-100 probes. In the first method the size distribution measured for

TABLE I. PARTICLE CONCENTRATION SUMMARY

AT TRANSMITTER SITE FOR 16 NOVEMBER 1978

TIME	PROBE	CONCENTRATION (p/cc) 2-47 MICRON	20-40 MICRON	20-320 MICRON	CONDITIONS
14:09	OAP-200X	----	12.96	14.84	Very light drizzle
14:15	FSSP-100	42.24	27.61	----	Heavy drizzle
14:37	OAP-200X	----	4.89	5.64	Heavy drizzle
14:51	FSSP-100	7.89	2.39	----	Heavy drizzle to light rain
15:33	FSSP-100	17.44	10.03	----	Heavy drizzle to rain
15:52	FSSP-100	16.15	8.73	----	Heavy drizzle to rain
17:06	FSSP-100	23.56	3.67	----	Misty (rain stopped)
17:40	FSSP-100	47.89	26.76	----	Heavy mist

TABLE II. EXTINCTION COEFFICIENTS, AEROSOL NUMBER DENSITY, MASS CONCENTRATION AND METEOROLOGICAL RANGE CALCULATED FOR TWELVE DIFFERENT CLOUD AEROSOL SIZE DISTRIBUTIONS

Time (hours)	Diameter Range (micron)	Extinction Coefficient (km^{-1})	Number Density ($\#/cm^3$)	Mass Concentration (g/m^3)	Meteorological Range (meters)
14:09	20-160	30.48	14.75	0.454	128.0
14:15	2-47	37.98	42.25	0.337	103.0
14:37	20-160	11.70	5.58	0.180	334.0
14:51	2-47	4.42	7.95	0.036	885.0
15:33	2-47	19.21	17.42	0.203	204.0
15:52	2-47	12.98	16.19	0.115	301.0
17:06	2-47	6.93	23.74	0.055	564.0
17:40	2-47	48.4	47.88	0.480	81.0
14:12	2-160	47.48	43.64	0.567	82.0
14:12	2-160	58.28	45.23	0.828	67.0
14:44	2-160	8.18	8.48	0.131	477.0
14:44	2-160	6.25	8.10	0.082	626.0

diameter ranges above 47 microns with the OAP-200X probe was combined with the size distribution measured for diameter ranges from 2 to 47 microns with the FSSP-100 probe. In the second method the size distribution measured for the diameter range above 47 microns was multiplied by the ratio of the number of aerosols measured in the 20-to-47-micron diameter range with the FSSP-100 probe to the number of aerosols measured in that range with the OAP-200X probe. Recall that the size distribution data that were combined were actually measured at slightly different times so that it would not be expected that they would give exactly the same number of aerosols in the diameter overlap range. Also, personnel at Sandia Laboratories indicated that they had a higher confidence in the accuracy of the size distribution measured with the FSSP-100 probe.

The cloud aerosol size distributions furnished by Sandia Laboratories are shown in Figures 1 through 4. The two size distributions for times 14:09 and 14:15 hours are shown in Figure 5. The two size distributions obtained by combining the measured distributions at times 14:37 and 14:51 are shown in Figure 6.

The normalized phase functions computed for each of the 12 different aerosol size distributions are shown in Figures 7 through 12. Note that although the cloud aerosol size distributions appear to vary quite radically over the time period during which the measurements were made, the normalized phase functions are very similar in shape. Probably the most significant difference in the phase functions, as far as the effect of the phase function on light transmission through the cloud is concerned, is the differences in the magnitudes of the forward scattering peaks. A small circle has been plotted in each of the figures at the peak of each of the phase functions to serve as an aid in locating the peak.

In addition to calculating the normalized phase function, the MIE-II program also computes the extinction coefficient for the collection of aerosols of a given size distribution. Other values given by the MIE-II program are the total aerosol number density (total number of aerosols per cubic centimeter) and the mass concentration (grams per cubic meter)

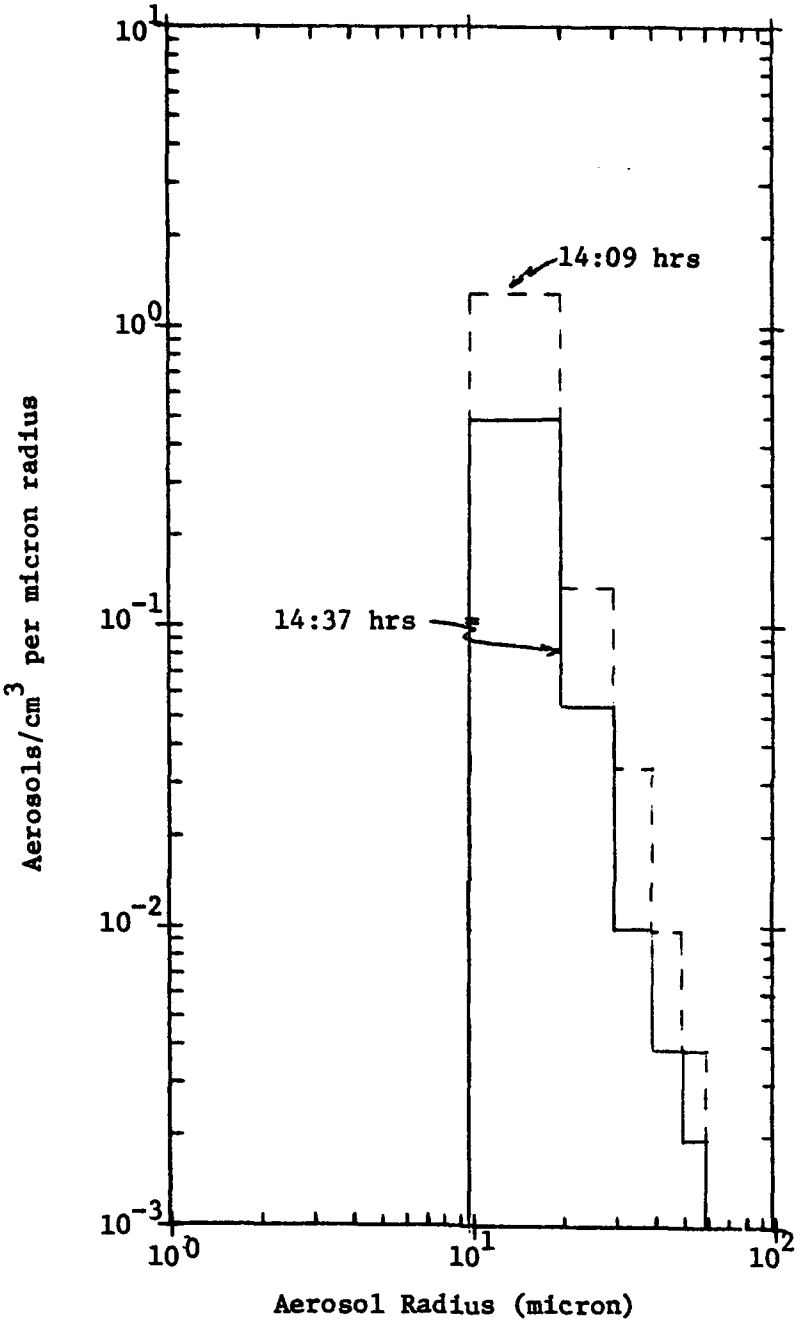

Fig. 1. Cloud Aerosol Size Distribution Measured with FSSP-100 Probe on Hawaii Island at 14:09 and 14:37 hours, 16 November 1978.

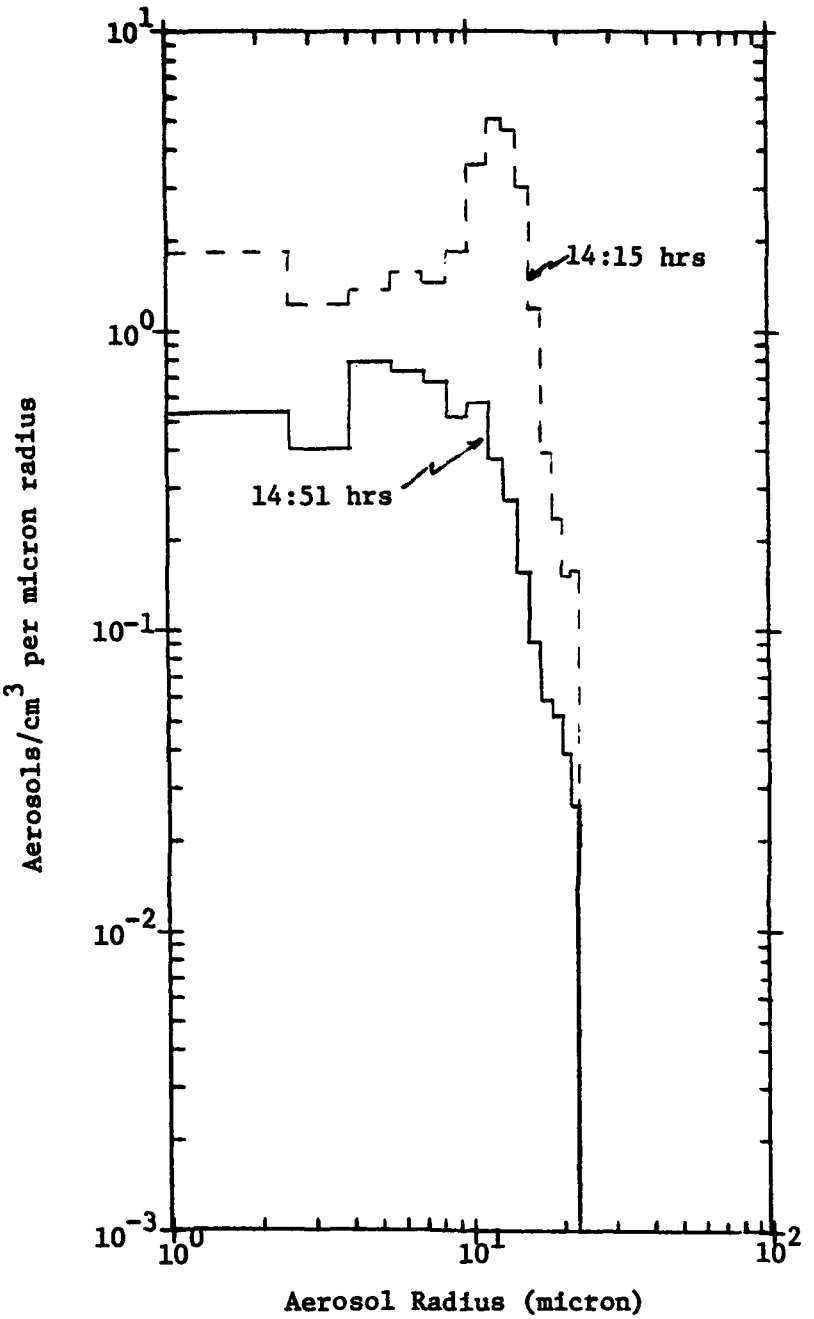

Fig. 2. Cloud Aerosol Size Distributions Measured with OAP-200X Probe on Hawaii Island at 14:15 and 14:51 hours, 16 November 1978.

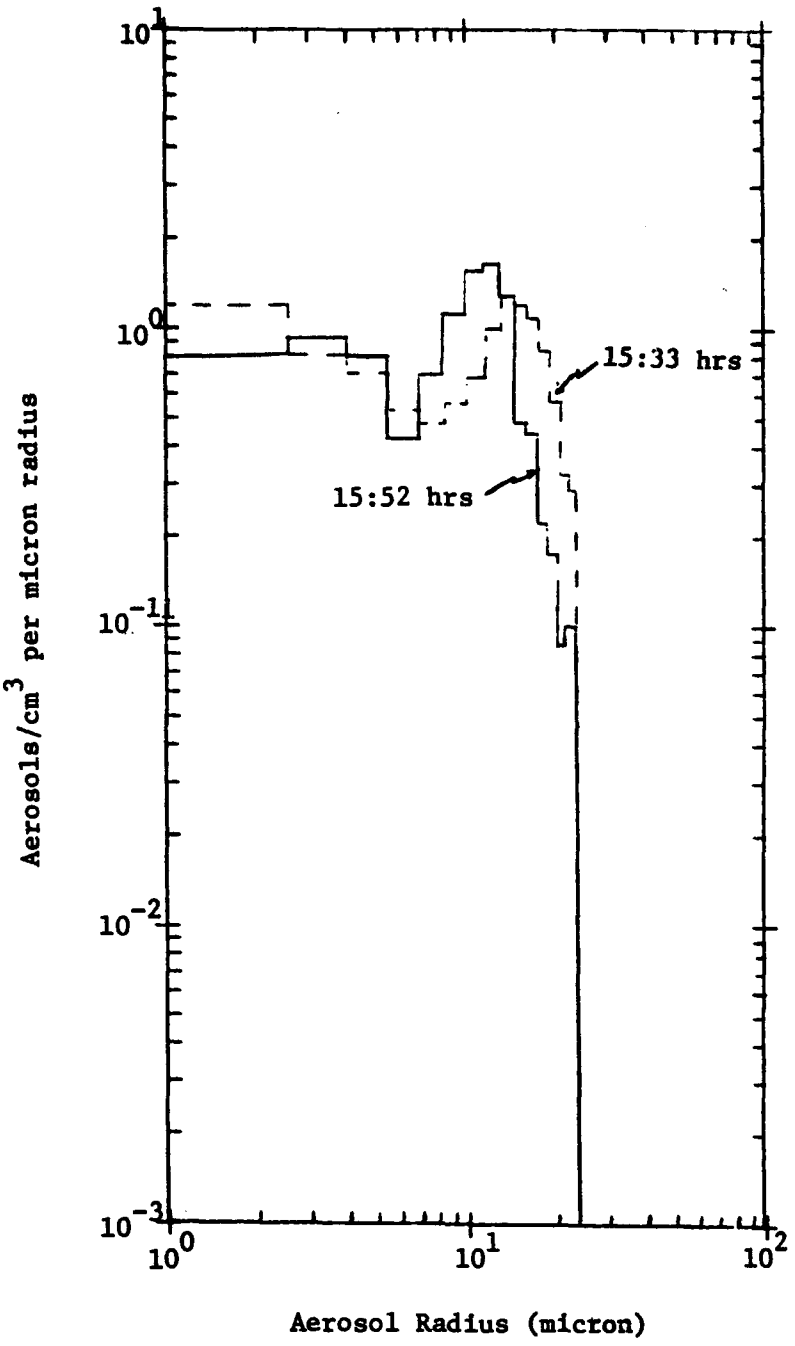

Fig. 3. Cloud Aerosol Size Distribution Measured with FSSP-100 Probe on Hawaii Island at 15:33 and 15:52 hours, 16 November 1978.

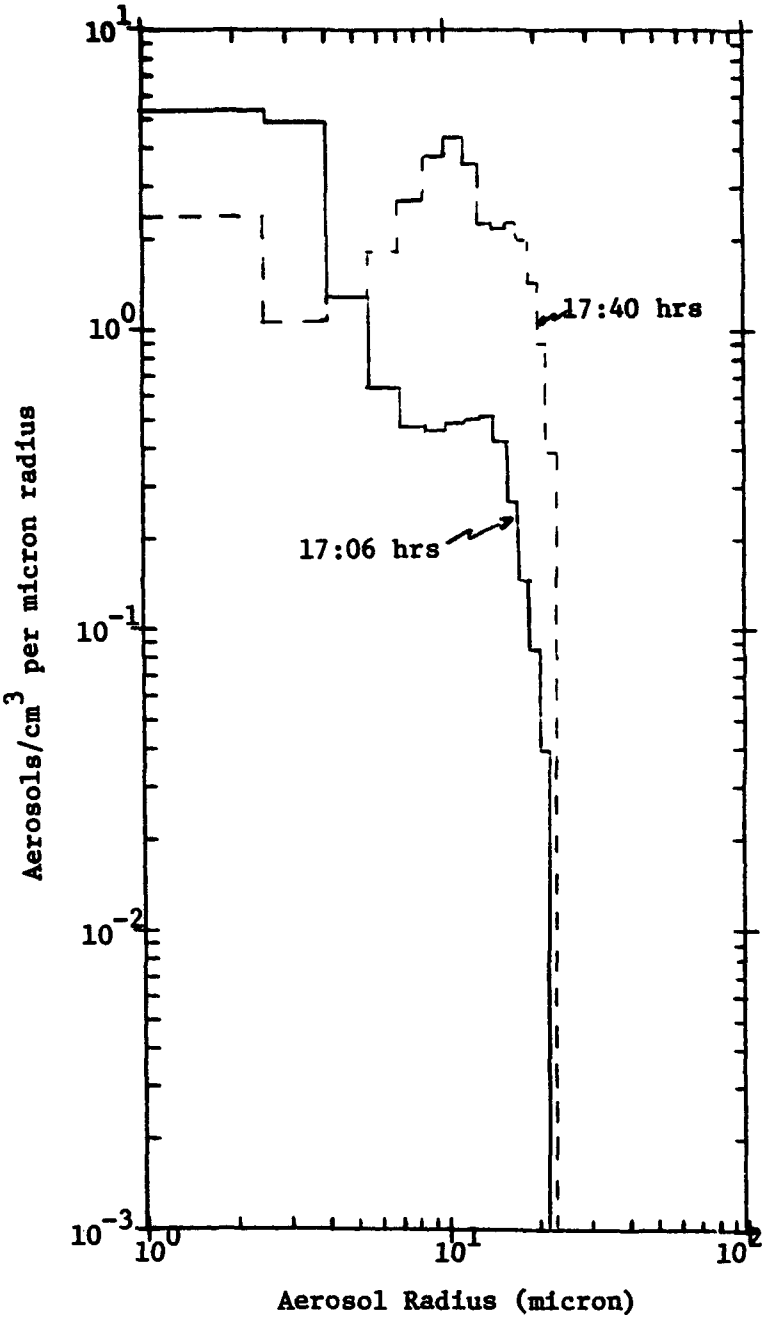

Fig. 4. Cloud Aerosol Size Distribution Measured with FSSP-100 Probe on Hawaii Island at 17:06 and 17:40 hours, 16 November 1978.

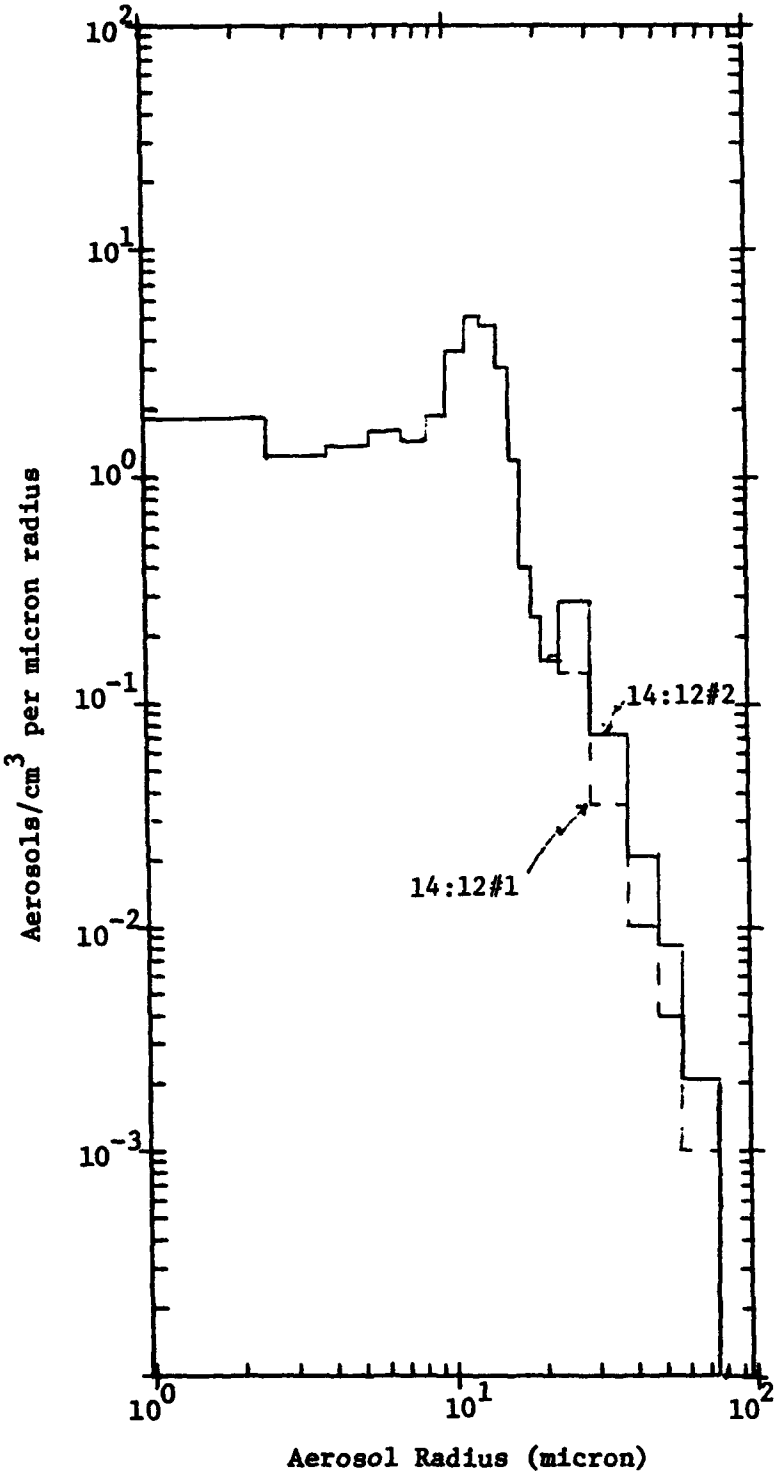

Fig. 5. Combined Aerosol Size Distribution Measured with OAP-200X and FSSP-100 Probes on Hawaii Island at 14:09 and 14:15 hours, 16 November 1978.

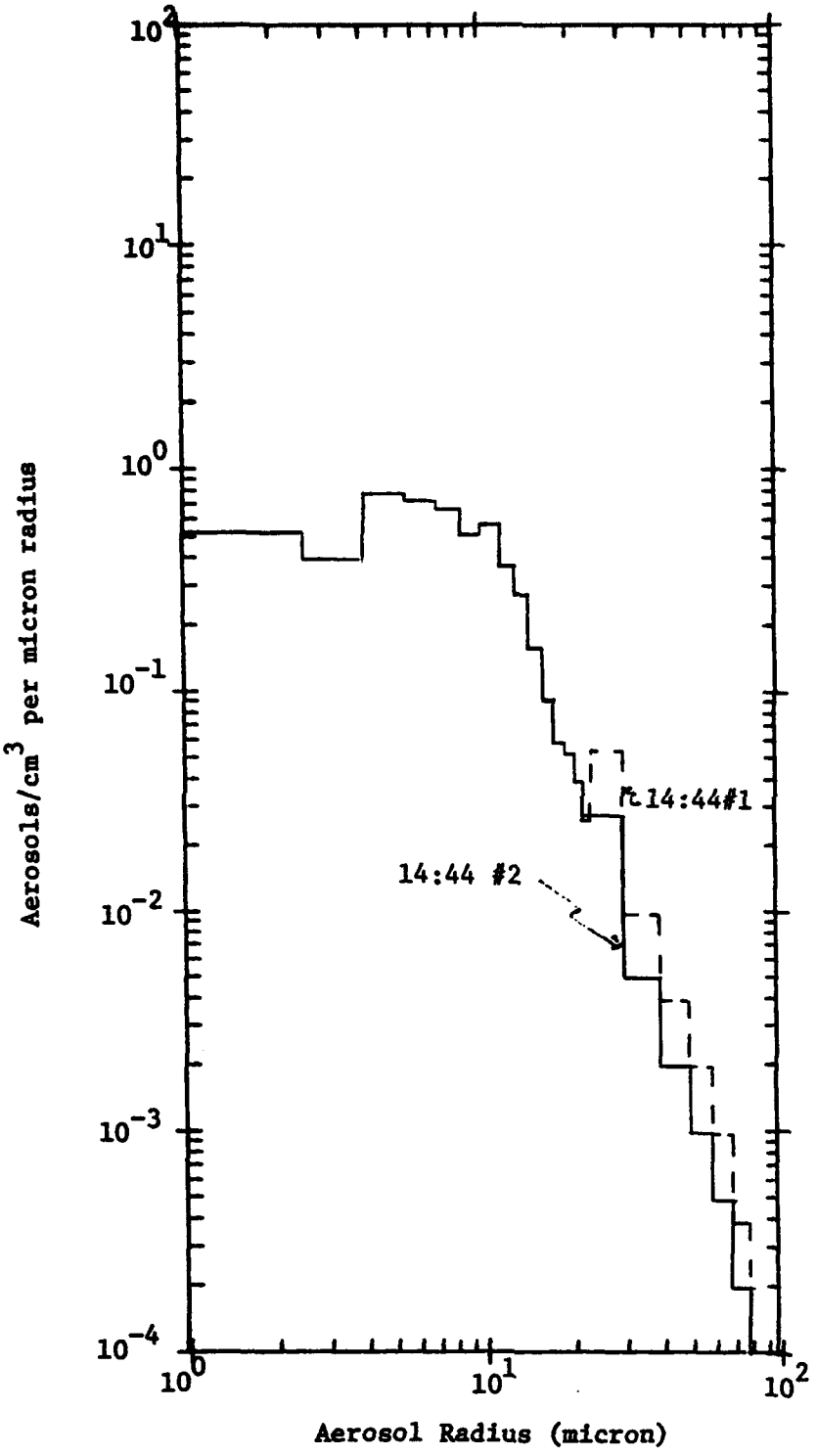

Fig. 6. Combined Aerosol Size Distribution Measured with OAP-200X and FSSP-100 Probes on Hawaii Island at 14:37 and 14:51 hours, 16 November 1978.

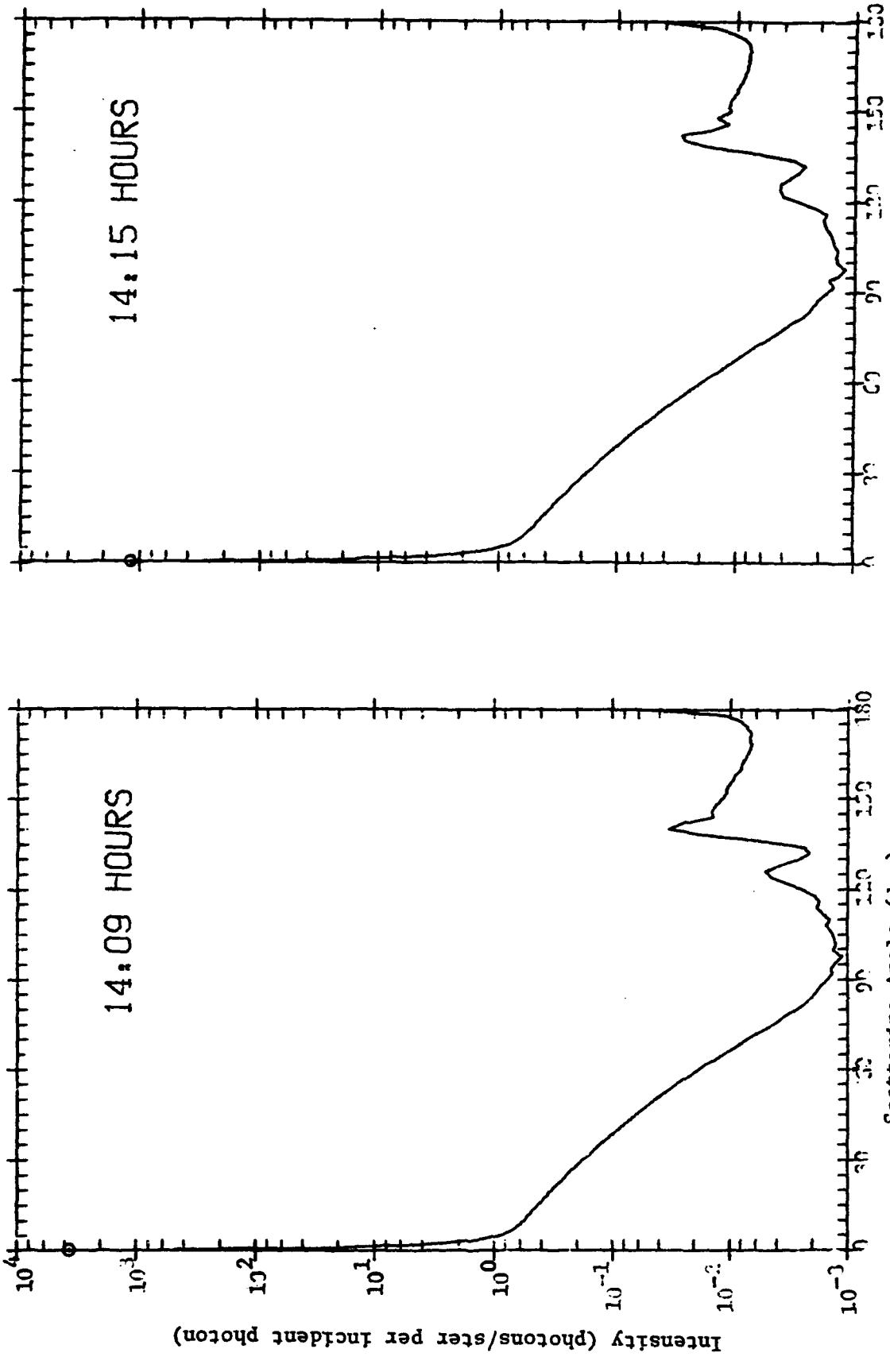

Fig. 7. Normalized Phase Functions for Cloud Aerosol Size Distributions Measured on Hawaii Island During 14:09 and 14:15 hours, 16 November 1978.

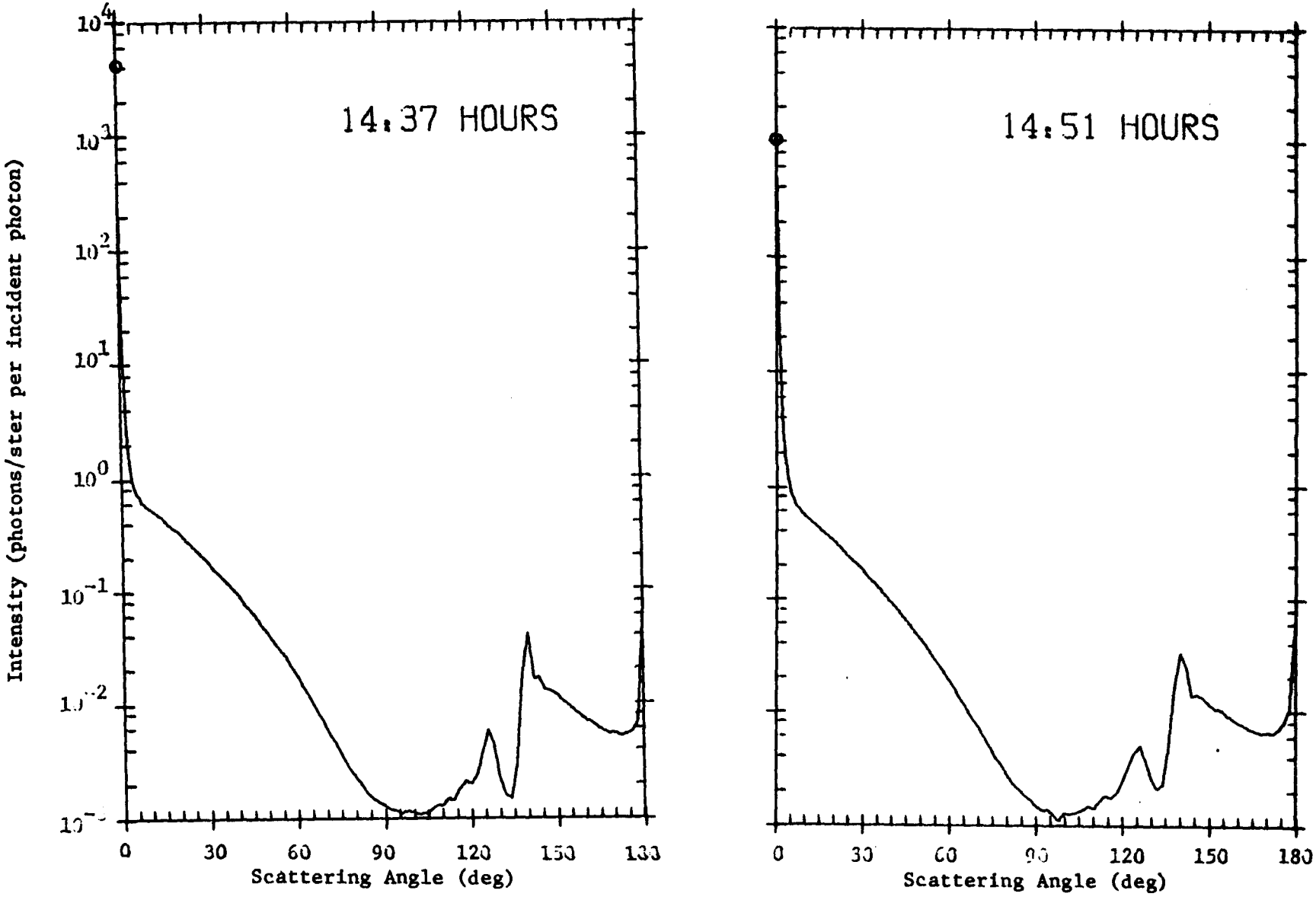

Fig. 8. Normalized Phase Functions for Cloud Aerosol Size Distributions Measured on Hawaii Island During 14:37 and 14:51 hours, 16 November 1978.

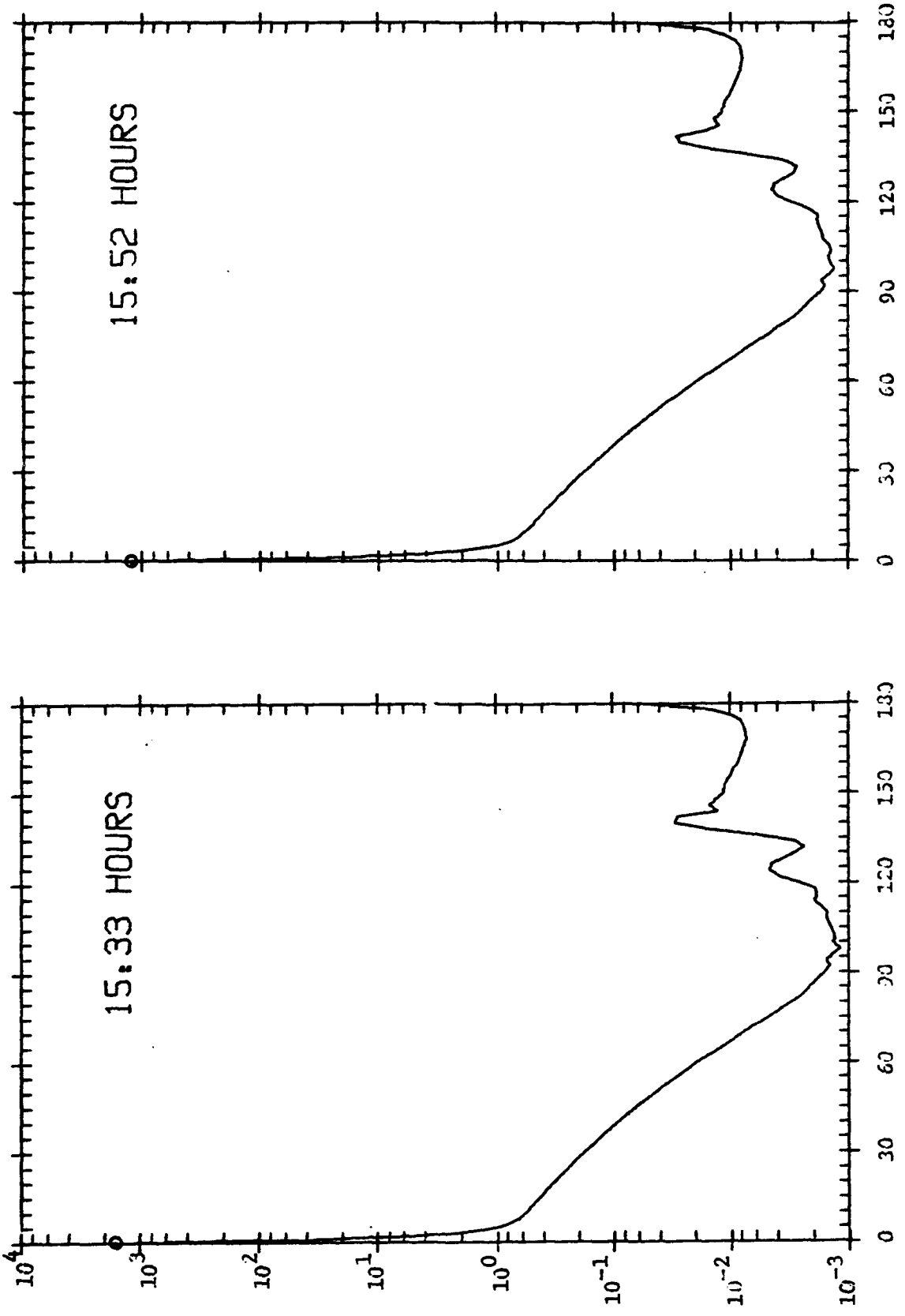

Fig. 9. Normalized Phase Functions for Cloud Aerosol Size Distributions Measured on Hawaii Island During 15:33 and 15:52 hours, 16 November 1978.

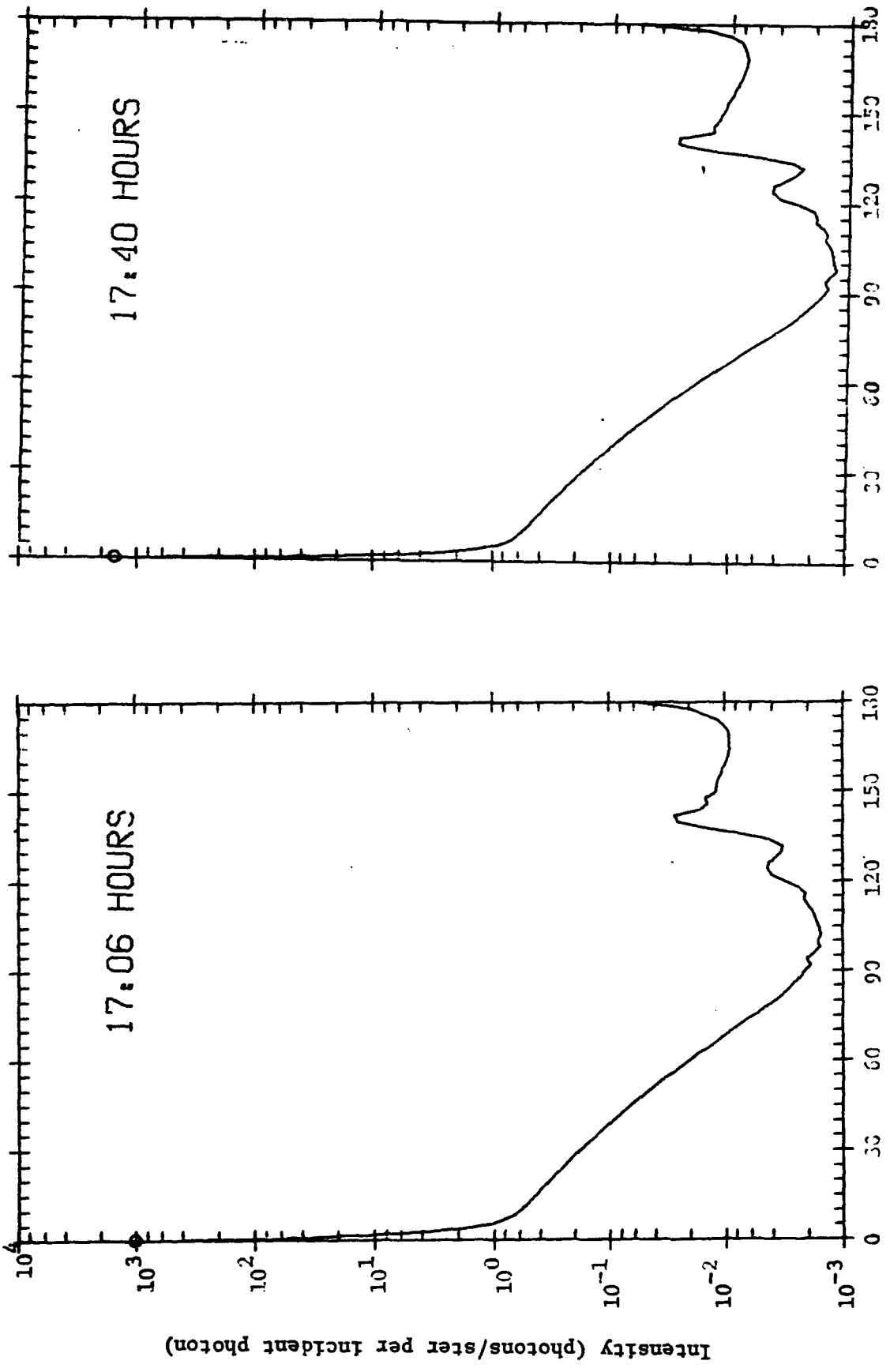

Fig. 10. Normalized Phase Functions for Cloud Aerosol Size Distributions Measured on Hawaii Island During 17:06 and 17:40 hours, 16 November 1978.

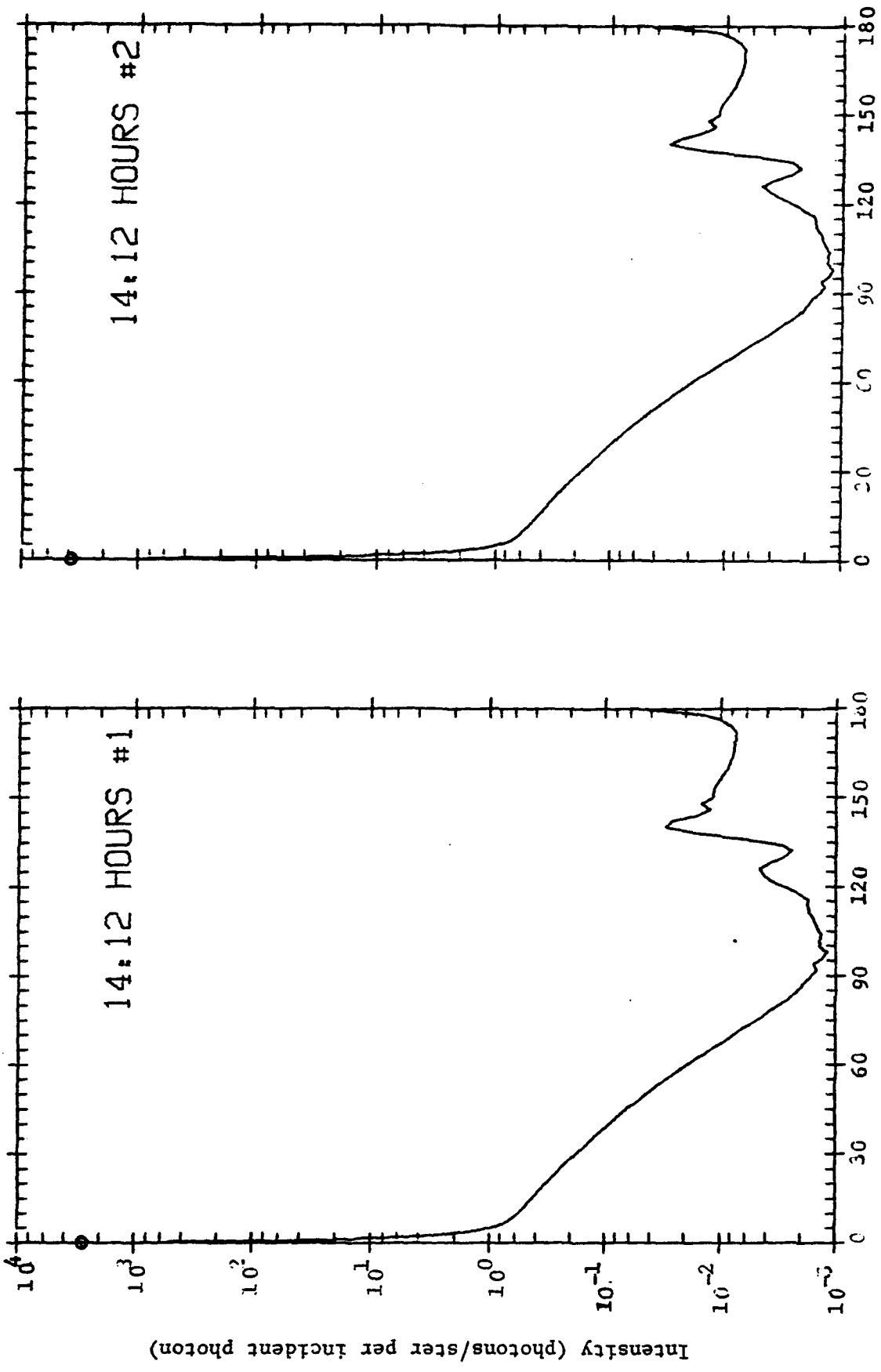

Fig. 11. Normalized Phase Functions for Combined Aerosol Size Distributions Measured on Hawaii Island During 14:09 and 14:15 hours, 16 November 1978.

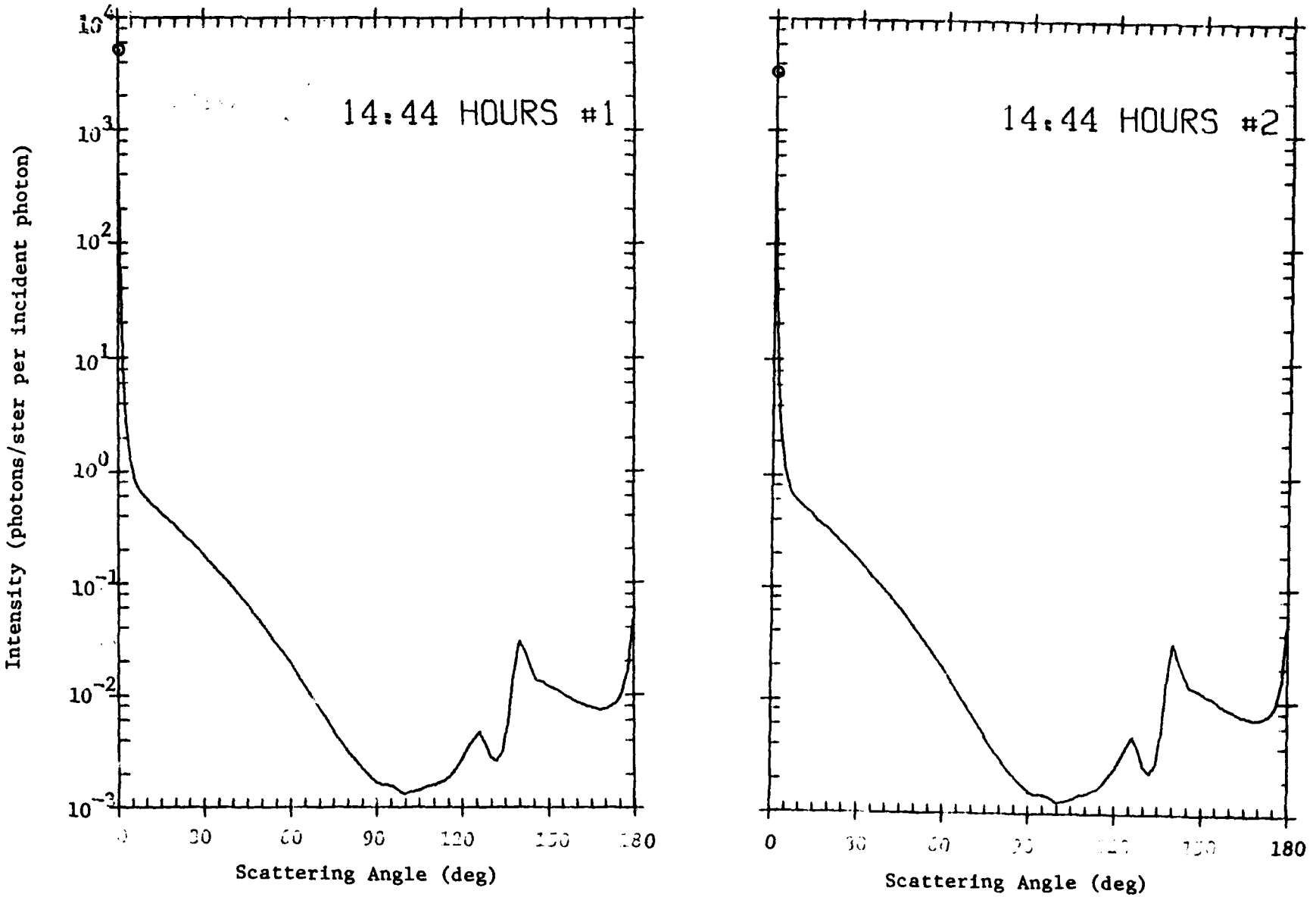

Fig. 12. Normalized Phase Function for Combined Aerosol Size Distribution Measured on Hawaii Island During 14:37 and 14:51 hours, 16 November 1978

for each of the aerosol size distributions considered. These values are listed in Table II for the twelve aerosol size distributions shown in Figures 1 through 6.

III. TIME-DELAY AND PULSE-STRETCHING CALCULATIONS

Time-delay and pulse-stretching calculations were performed for two of the twelve cloud models discussed in the previous section of this report. The two models selected for study were the models for times 15:33 and 17:06 hours. These two cloud models give optical distances of 14.7 and 5.3, respectively, between a source and receiver separated by a distance of 765 meters. The time-dependant responses for 18 source-receiver orientations were computed for each of the two cloud models. These responses were computed using the TPART-III Monte Carlo Program assuming an instantaneous emitting source. Then a Gaussian pulse 10 nanoseconds wide at half maximum was convolved with the time-dependent responses calculated with TPART-III to give the time responses for the 10 nanosecond wide gaussian pulse. The various source and receiver orientations considered are listed in Tables III and IV along with a summary of the calculations. The source and receiver angles referred to in the tables are the polar angles measured from the source-receiver axis. For the calculations, the source-receiver axis was oriented horizontally and located 25 meters above the ground surface. When the laser beam or the receiver field-of-view was scanned off the source-receiver axis, it was scanned vertically above the source-receiver axis. In TPART-III the clouds were assumed to be 450 meters in thickness and to extend from the ground surface to the 450 meter altitude.

Tables III and IV give a summary of the results of the calculations. The time-integrated receiver response to the direct radiation, and the single and multiple-scattered radiation are given for the 18 combinations of the three source and six receiver elevations. The units of the calculated direct, single-scattered, multiple-scattered, and total-scattered responses are photons incident upon the receiver within a 1 degree field-of-view per photon emitted from the source. Recall that the receiver disk is an annular ring having a 4.5 inch inside diameter and a 7 inch outside diameter, thus the receiver surface is 890.54 square centimeters in area. The peak power is the amplitude of the received pulse obtained after convolving a gaussian pulse 10 nanoseconds wide at half maximum with the

TABLE III. CALCULATED TIME INTEGRATED RESPONSES FOR OPTICAL DISTANCE OF 5.3

SOURCE ANGLE	RECEIVER ANGLE	DIRECT RESPONSE	SINGLE SCATTERED RESPONSE	MULTIPLE SCATTERED RESPONSE	TOTAL RESPONSE	PEAK POWER	TIME DELAY (NSEC)	PULSE WIDTH (NSEC)
0	0	3.7-03	3.0-04	1.3-05	4.0-03	1.4+04	1.0	10.06
	1		3.1-06	1.2-06	4.4-06	2.6+01	1.0	10.06
	2		1.3-06	1.3-07	1.4-06	1.1+01	1.0	10.06
	3		4.3-07	2.7-08	4.6-07	4.4+00	1.0	10.07
	5			4.0-09	4.0-09			
	10			1.4-09	1.4-09	6.2-02	2.6	10.89
5	0		5.2-10	2.7-09	3.2-09	1.2-01	1.8	10.55
	1		8.2-10	4.0-09	4.9-09	3.7-01	2.8	10.35
	2		6.8-10	2.5-09	3.2-09	2.5-01	4.0	10.47
	3		5.7-10	2.3-09	2.9-09	2.3-01	6.0	10.48
	5		5.2-10	2.1-09	2.6-09	2.1-01	10.0	10.77
	10		2.5-10	2.7-09	3.0-09	2.2-01	19.2	11.04
10	0		1.2-10	6.1-10	7.3-10	3.5-02	1.8	10.61
	1		2.2-10	7.7-10	9.9-10	7.7-02	4.8	10.74
	2		2.0-10	1.1-09	1.3-09	1.0-01	9.2	10.93
	3		2.0-10	8.6-10	1.1-09	7.2-02	12.0	11.18
	5		1.5-10	7.1-10	8.7-10	6.0-02	20.0	11.43
	10		1.4-10	4.4-10	5.8-10	3.2-02	39.2	12.81

TABLE IV. CALCULATED TIME INTEGRATED RESPONSES FOR OPTICAL DISTANCE OF 14.7

SOURCE ANGLE	RECEIVER ANGLE	DIRECT RESPONSE	SINGLE SCATTERED RESPONSE	MULTIPLE SCATTERED RESPONSE	TOTAL RESPONSE	PEAK POWER	TIME DELAY (NSEC)	PULSE WIDTH (NSEC)
0	0	3.0-07	1.8-09	3.1-08	3.3-07	1.8+00	1.0	10.06
	1			9.0-09	9.0-09	7.4-02	1.8	10.98
	2			6.1-11	6.1-11	1.3-03	1.8	10.67
	3			4.5-11	4.5-11	1.2-03	2.6	11.54
	5			4.9-11	4.9-11	2.3-03	2.0	10.46
	10			2.8-11	2.8-11	8.7-04	4.2	10.80
5	0		9.7-14	8.5-11	8.5-11	2.2-03	28.2	10.39
	1		1.5-13	6.2-11	6.2-11	3.2-03	4.0	10.37
	2		1.3-13	8.1-12	8.2-12	3.4-04	4.8	11.44
	3		9.5-14	2.3-11	2.3-11	9.8-04	7.0	10.46
	5		5.4-14	2.8-11	2.8-11	1.3-03	10.0	10.78
	10			2.0-11	2.0-11	4.2-04	18.8	11.88
10	0		2.7-14	8.2-12	8.2-12	2.1-04	12.0	10.86
	1		4.8-14	5.2-12	5.2-12	1.6-04	6.4	11.62
	2		4.5-14	4.9-12	5.0-12	6.1-05	9.6	13.36
	3		4.6-14	8.4-12	8.5-12	3.4-04	14.4	11.19
	5		3.6-14	1.6-11	1.6-11	4.4-04	19.6	12.54
	10		7.6-14	7.3-12	7.4-12	2.1-04	39.2	13.98

time-dependant transmission data calculated with the TPART-III program. The initial gaussian pulse integrated over time is equal to unity so the peak power of the initial pulse emitted from the source is $9.39 * 10^{9}$ photons per second. The units of the peak power in Tables III and IV are photons per second incident upon the receiver surface within a 1 degree field-of-view per photon emitted from the source. The time delay is the time at which the peak power is received minus the time of the peak power in the direct pulse. Even though a direct pulse is not calculated unless both the source and receiver are focused on the source-receiver axis, it is assumed that the time of the direct pulse is equal to the time of the peak emission plus the time required for light to traverse the distance between the source and receiver positions. The pulse width is the width of the observed pulse at half maximum.

Only in those cases where the laser beam is oriented along the source-receiver axis in the cloud that has a 5.3 optical source-receiver separation distance does the single-scattering response exceed the multiple-scattering response. No single-scattering responses were calculated for the receiver elevations of 5 and 10 degrees for this case. No single-scattering responses were calculated for the case where the source beam was oriented along the source-receiver axis in the cloud having a 14.7 optical source-receiver separation distance when the receiver field-of-view was elevated from the source-receiver axis. The most logical explanation for this failure to compute single-scattered responses is that for these cases the scattering volume formed by the intersection of the laser beam and the receiver field-of-view is extremely small and is located at large optical distances from the source so that the likelihood of sampling first order collisions within that volume is extremely small.

One TPART-III problem was run for each source-receiver orientation in each of the two cloud models. In each TPART-III problem 5000 histories were run to determine the data in Tables III and IV. Histories were terminated when the photon weight dropped below $1.0 * 10^{-5}$ or when the number of collisions exceeded 100 for the 5.3 source-receiver optical separation distance or 150 for the 14.7 source-receiver optical separation distance.

The receiver responses were computed for the scattered radiation arriving at the receiver over a period of 60 microseconds in retarded time. Retarded time is defined to be the actual time required for a photon to traverse its random path between the source and receiver positions minus the time that would have been required for it to traverse the direct path between the source and receiver positions. In the problems run for the 5.3 source-receiver optical separation distance an average of 131 histories out of 5000 run were terminated after having undergone a maximum of 100 collisions. The remainder of the 5000 histories were terminated by the weight cut-off mechanism. That is, histories were terminated whenever the weight of the photon dropped below the minimum weight cut-off of $1.0 * 10^{-5}$. The average number of collisions per history was approximately 36. In the problems run for the 14.7 source-receiver optical separation distance, an average of 277 histories out of 5000 were terminated after having undergone a maximum of 150 collisions. The remainder of the 5000 histories were terminated by the weight cut-off mechanism. The average number of collisions per history for these problems was approximately 63. Since there was no absorption allowed in the two cloud models, there were only two processes which were used to reduce the photon weight and to eventually cause the photon histories to terminate on the minimum weight cut-off. These two processes were: 1) a weight reduction when the photon reflected from the ground surface and 2) a weight reduction when the photon was forced to remain within the cloud so that it could not escape through the top of the cloud. Thus the histories terminated by weight reduction actually represent those photons that were either absorbed in the ground material or escaped from the top of the cloud.

The calculated time integrated receiver responses as a function of the order of scatter were printed as a portion of the TPART-III output. These responses were accumulated as a function of the order of scatter and divided by the total response summed over all orders of scattering to give an indication of the number of scatters that must be considered in order to determine the total multiple-scattering contribution. These data are plotted in Figures 13 through 18 for the first 50 orders of scattering.

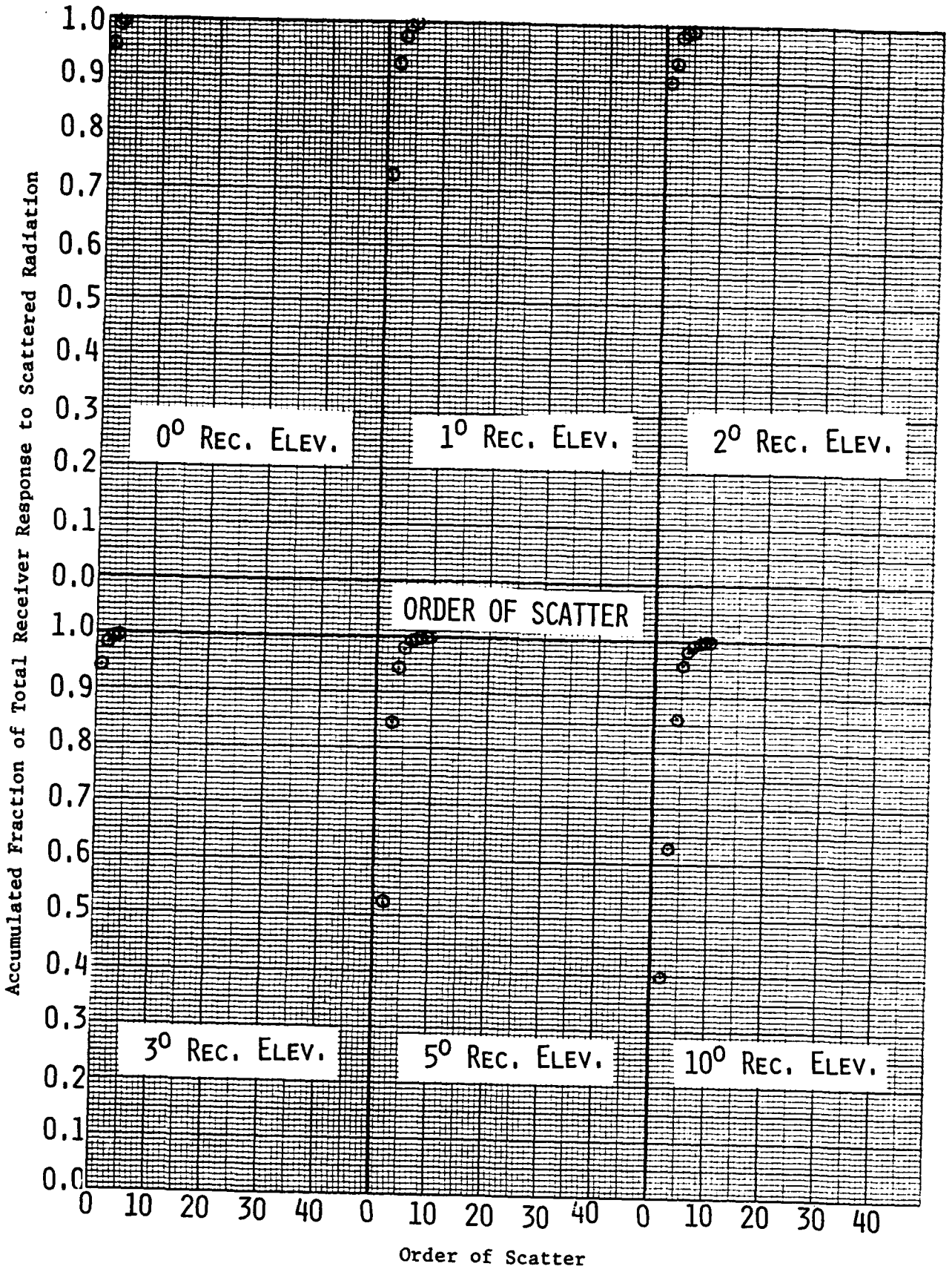

Fig. 13. Fractional Receiver Response Accumulated Versus Order of Scatter, 0° Source Elevation, 5.3 Source-Receiver Optical Separation Distance.

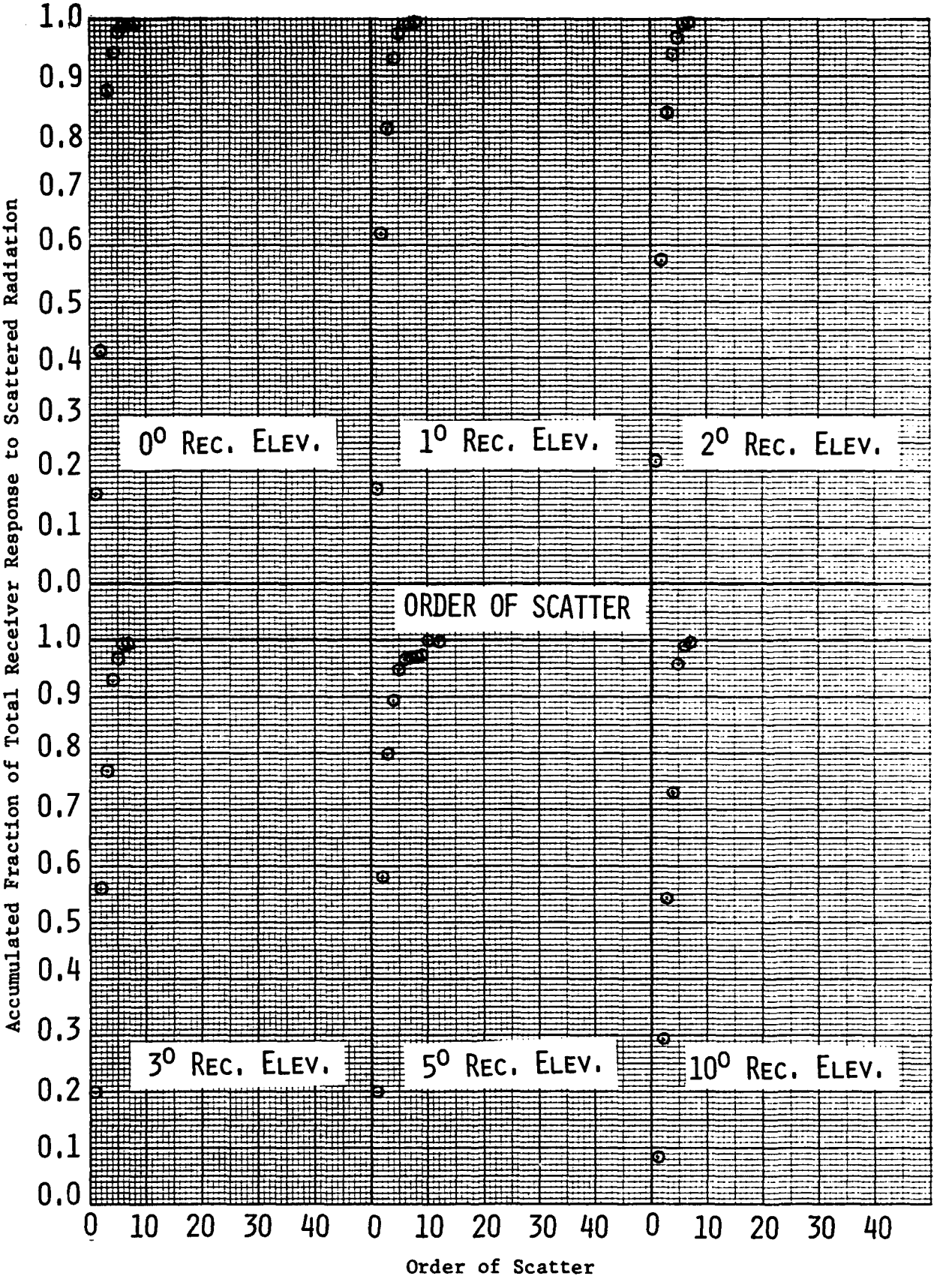

Fig. 14. Fractional Receiver Response Accumulated Versus Order of Scatter, 5° Source Elevation, 5.3 Source-Reciver Optical Separation Distance.

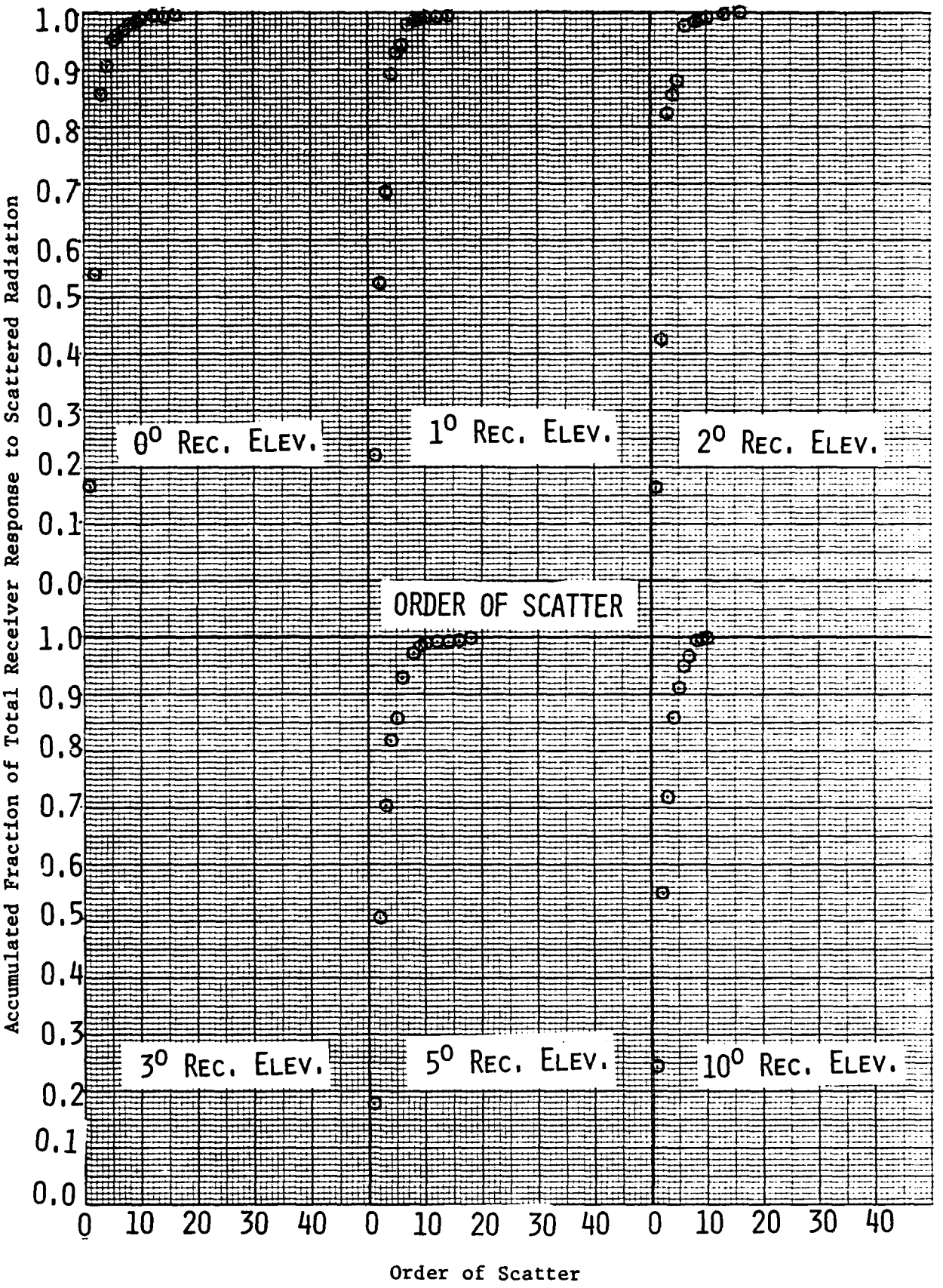

Fig. 15. Fractional Receiver Response Accumulated Versus Order of Scatter, 10° Source Elevation, 5.3 Source-Receiver Optical Separation Distance.

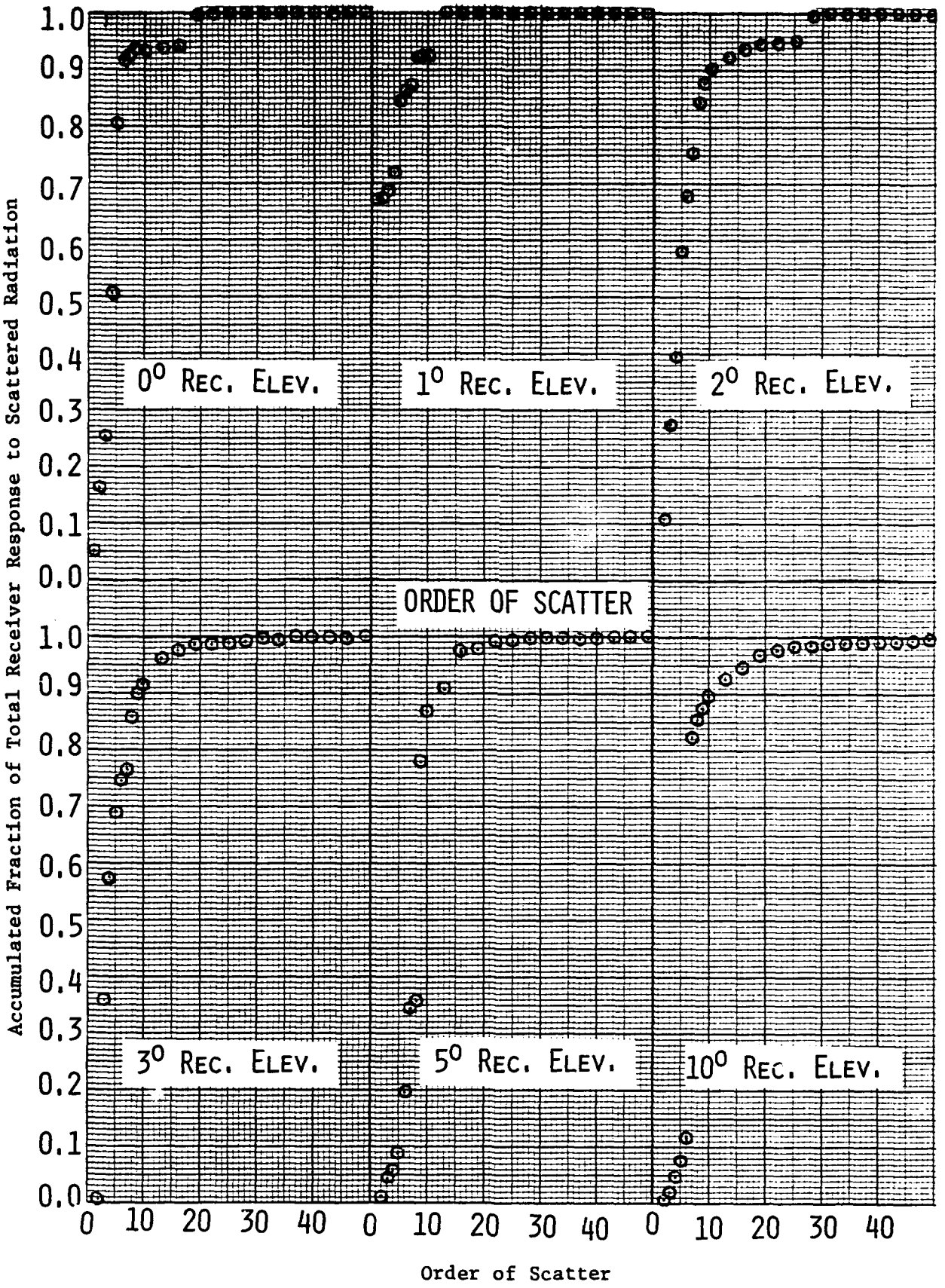

Fig. 16. Fractional Receiver Response Accumulated Versus Order of Scatter, 0° Source Elevation, 14.7 Source-Receiver Optical Separation Distance.

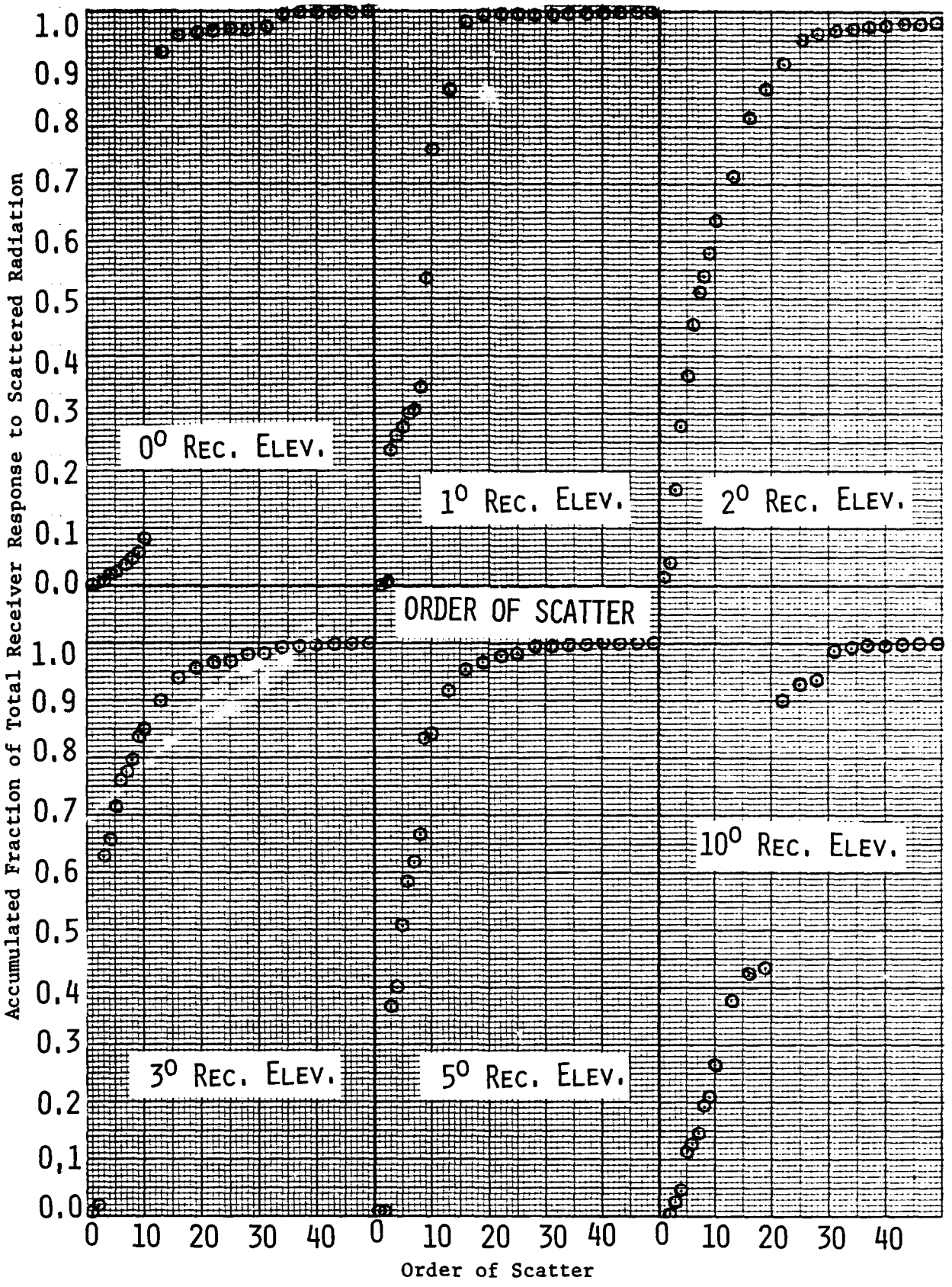

Fig. 17. Fractional Receiver Response Accumulated Versus Order of Scatter, 5° Source Elevation, 14.7 Source-Receiver Optical Separation Distance.

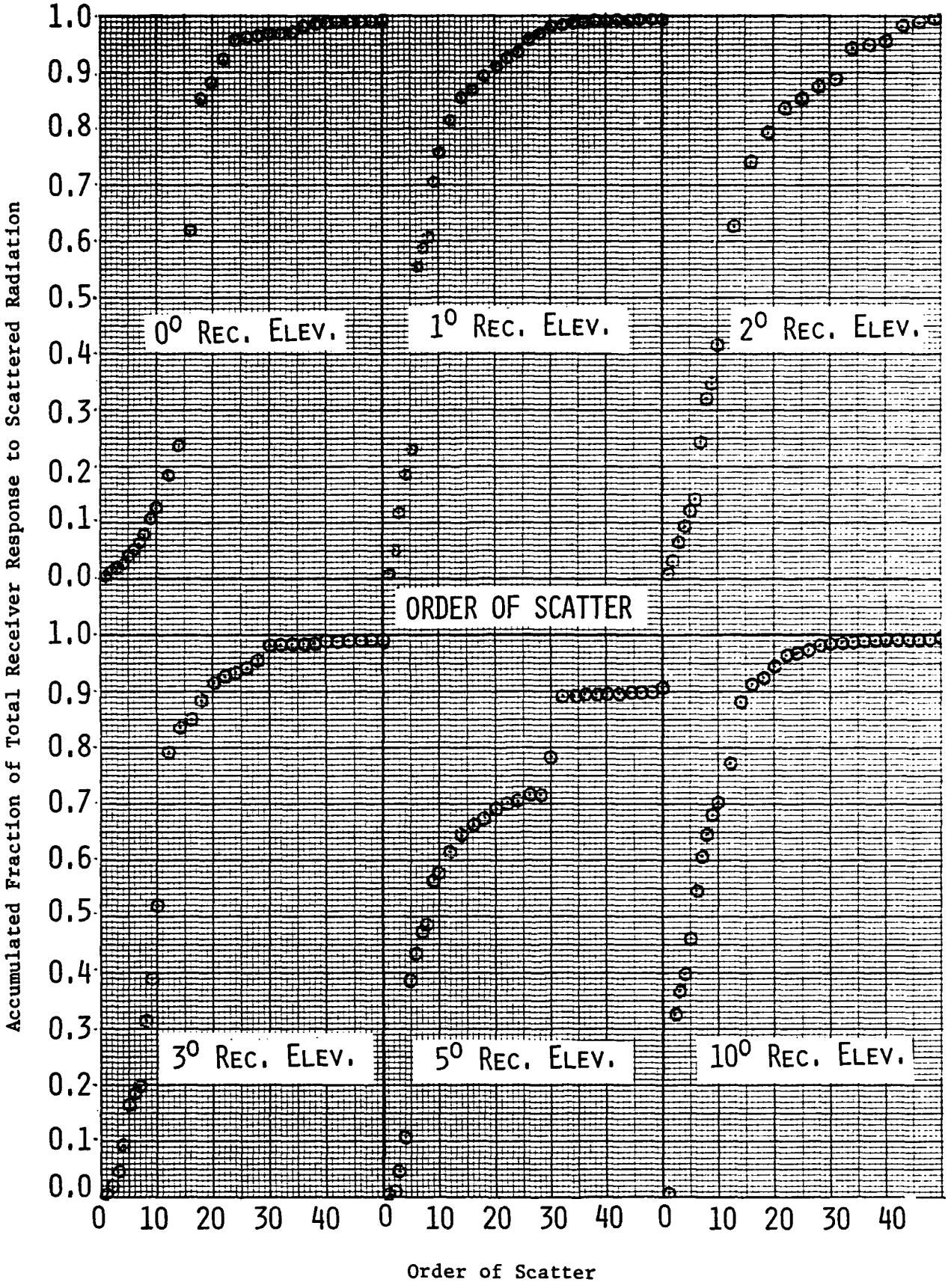

Fig. 18. Fractional Receiver Response Accumulated Versus Order of Scatter, 10° Source Elevation, 14.7 Source-Receiver Optical Separation Distance.

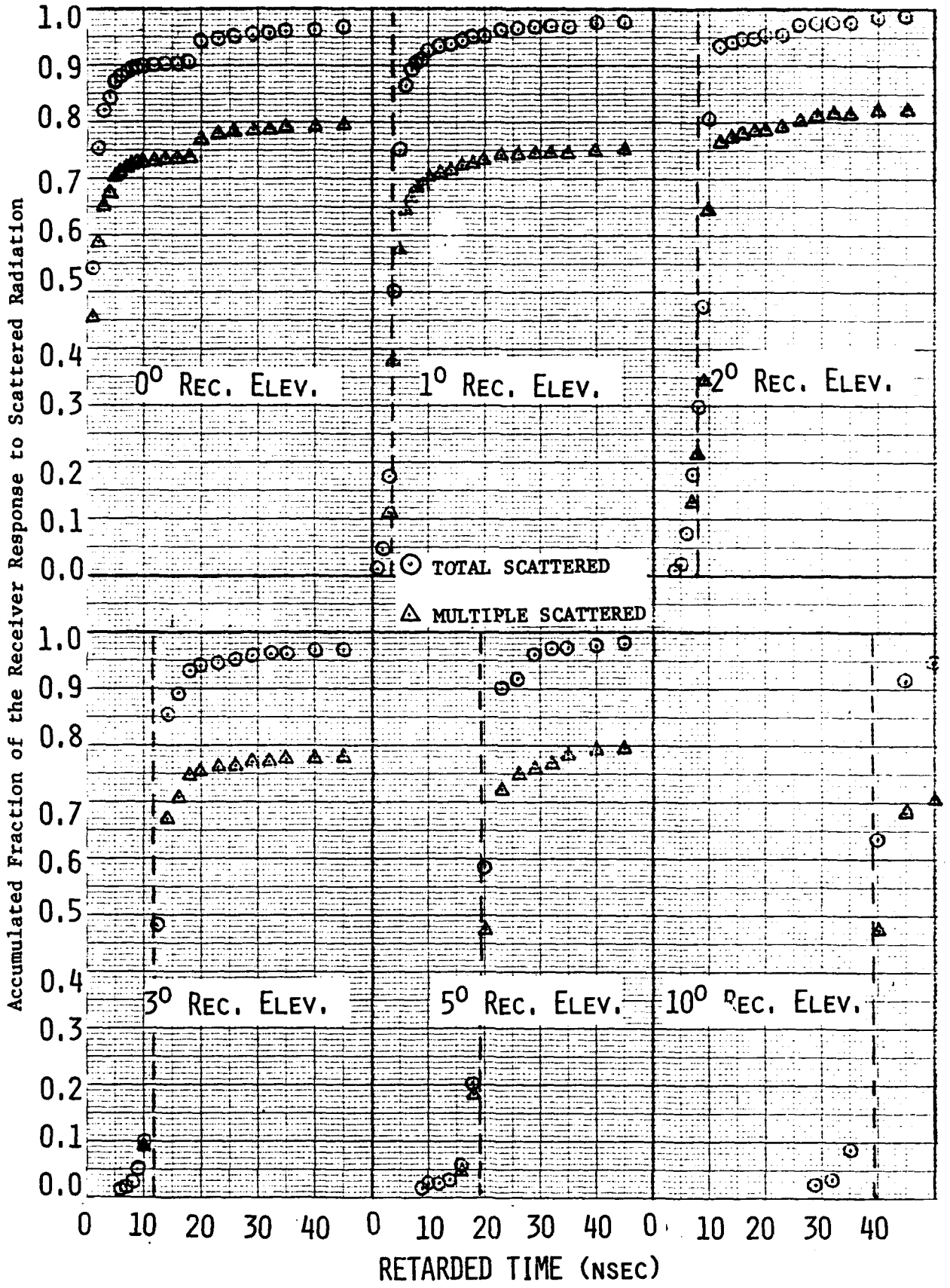

Fig. 20. Fractional Receiver Response Accumulated Versus Retarded Time, 10° Source Elevation, 5.3 Source-Receiver Optical Separation Distance.

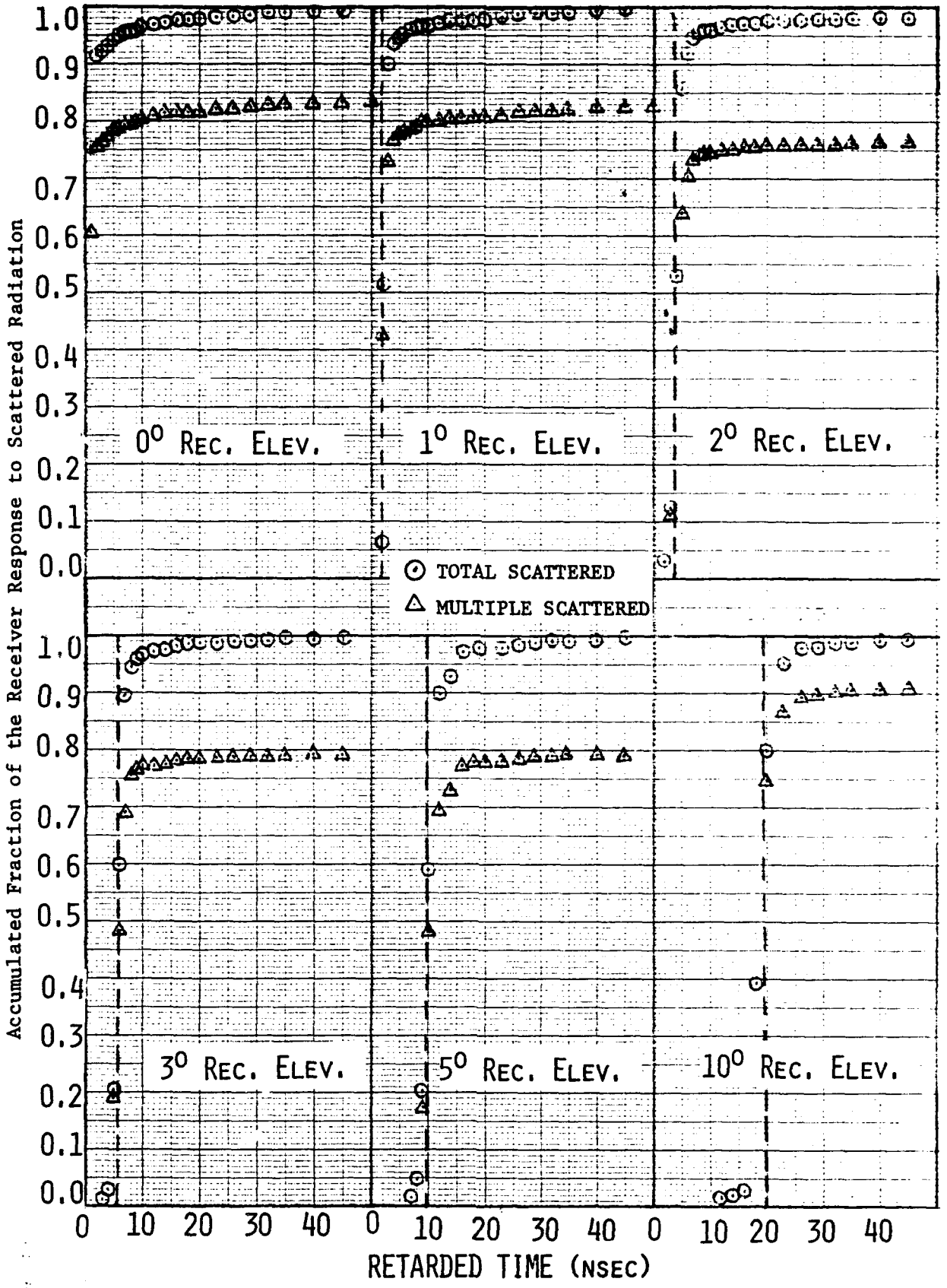

Fig. 19. Fractional Receiver Response Accumulated Versus Retarded Time, 5° Source Elevation, 5.3 Source-Receiver Optical Separation Distance.

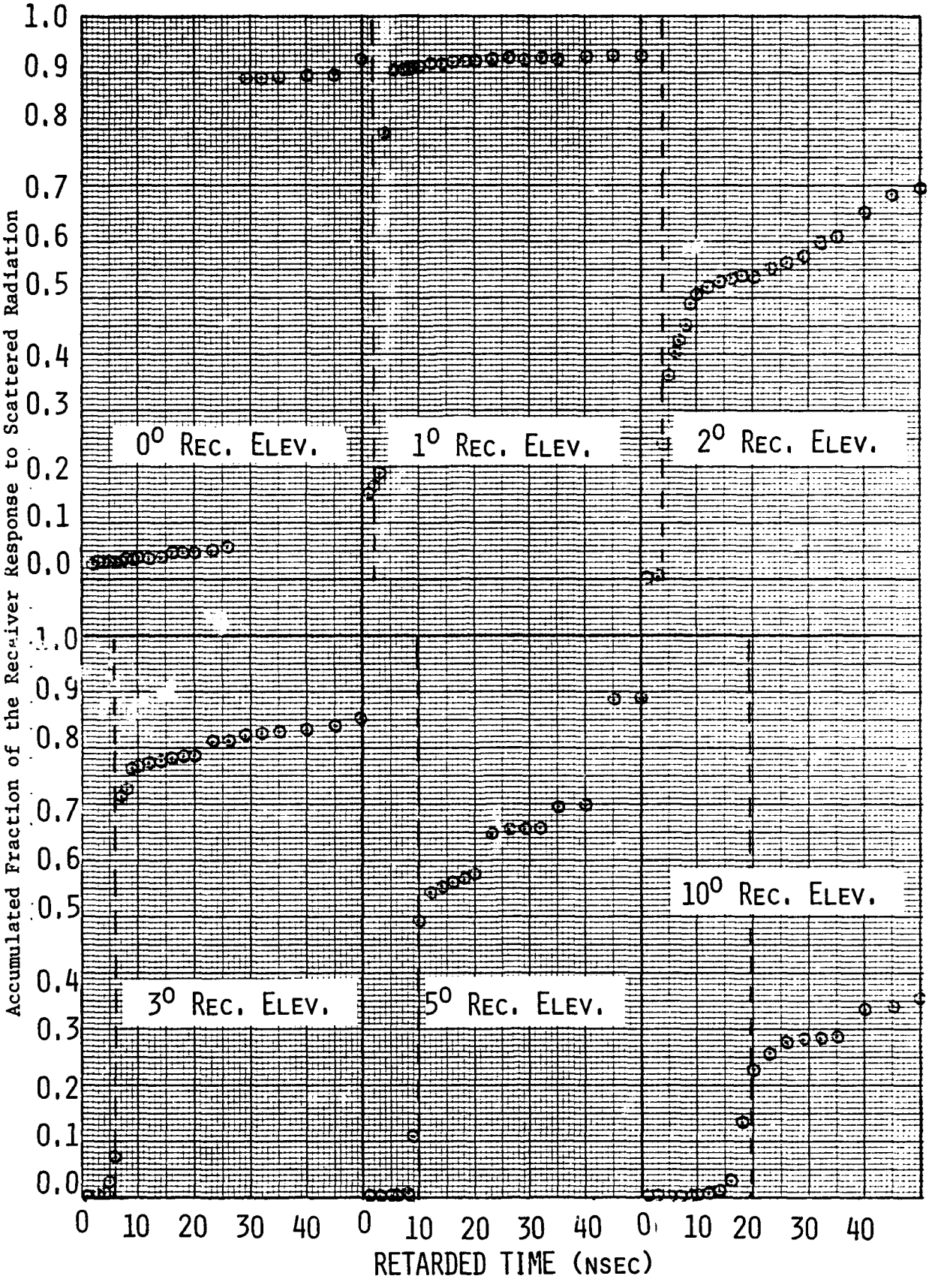

Fig. 21. Fractional Receiver Response Accumulated Versus Retarded Time, 5° Source Elevation, 14.7 Source-Receiver Optical Separation Distance.

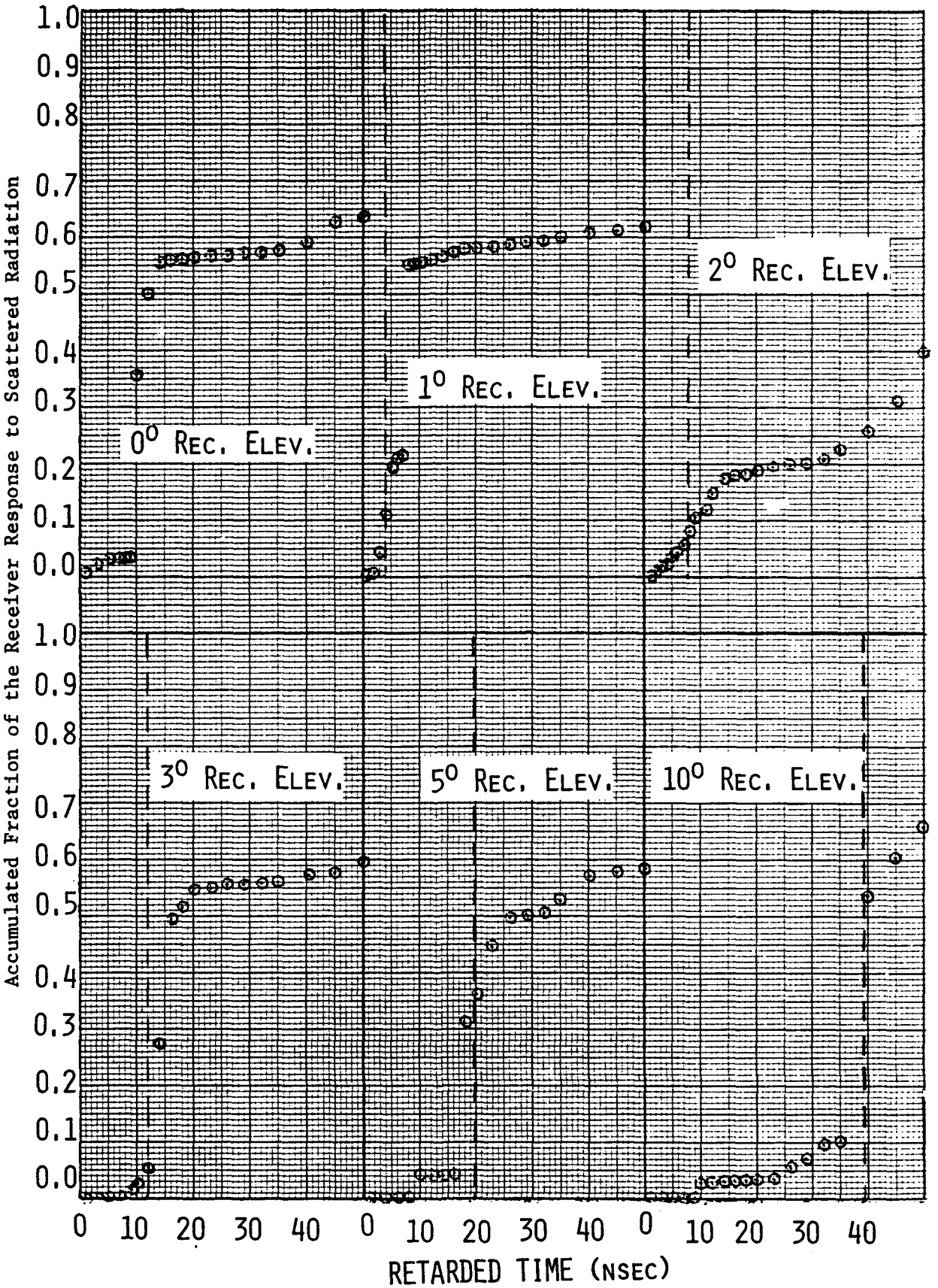

Fig. 22. Fractional Receiver Response Accumulated Versus Retarded Time, 10° Source Elevation, 14.7 Source-Receiver Optical Separation Distance.

for the 5.3 source-receiver optical separation distance this sharp increase occurs in the cumulative distributions for both the total and multiple-scattered radiation. Single scattering for the 14.7 source-receiver optical separation distance was such a small portion of the total scattered radiation that the cumulative time distributions for the total and multiple scattering are almost identical. Even though the single-scattering contributions for the 14.7 source-receiver optical separation distance were insignificant, the sharp rises in the cumulative distributions occur at almost the exact times that the single-scattered radiation arrives at the receiver. The sharp rises in the cumulative time distribution of the multiple-scattered radiation for the 5.3 source-receiver optical separation distance also occur at almost the exact time that the single-scattered radiation arrives at the receiver. Due to the high degree of collimation of the source and receiver, the single-scattered contribution is limited to a very short time period (2 or 3 nanoseconds) centered at the time given by the formula:

$$T = D(((\sin\alpha + \sin\beta)/\sin(\alpha+\beta)) - 1.0)/V$$

where D is the source-receiver separation distance, V is the velocity of light, and α and β are the elevation angles of the source beam and the receiver field-of-view, respectively. Table V lists the times of arrival of the single-scattered response for the various combinations of source and receiver elevation angles. These times are indicated in Figures 19 through 22 with the vertical dashed lines.

The fact that the sharp increases in the cumulative time distributions of the multiple-scattered radiation occur during the same time periods that the single-scattered radiation reaches the receiver indicates that a large portion of the multiple-scattered radiation is scattering in the forward direction along the beam and that the light intensity is concentrated along the original direction of the beam even after several orders of scatter. Note in Figures 19 and 20 for the 5.3 source-receiver optical separation distance that 95 percent or more of the total scattered radiation had been received within the first 50 nanoseconds of retarded time. Most of that radiation was received

TABLE V. SINGLE-SCATTERING RETARDED TIMES VERSUS SOURCE AND RECEIVER ELEVATION ANGLES

Source Elevation (deg)	Receiver Elevation (deg)	Time of Single-Scattered Response (nanosecond)
0	0	0
	1	0
	2	0
	3	0
	5	0
	10	0
5	0	0
	1	1.94
	2	3.89
	3	5.84
	5	9.74
	10	19.56
10	0	0
	1	3.40
	2	7.80
	3	11.71
	5	19.56
	10	39.34

during a few nanoseconds time period centered about the time that the first order scattered radiation reached the receiver. In Figures 21 and 22 showing the fraction of the total scattered radiation accumulated as a function of time for the 14.7 source-receiver optical separation distance, it is seen that only from 30 to 80 or 90 percent of the scattered radiation arrives at the receiver position within the first 50 nanoseconds of retarded time. Plots of the data for longer time periods show in general that there is a gradual increase in the cumulative distribution at times greater than 50 nanoseconds and a time period in the order of a few microseconds is required to obtain 93 to 99 percent of the total scattered radiation. Even for the 14.7 source-receiver optical separation distance, the multiple-scattered radiation that arrives at the receiver during the same time period that the single-scattered radiation arrives makes up a significant portion of the total scattered radiation at the receiver.

The time distributions of the scattered radiation computed for an instantaneous emitting source using the TPART-III program were convolved with a gaussian pulse that was 10 nanoseconds wide at half maximum. The source pulse was assumed to peak at time $t = 0$ and was defined over a time period ranging from -15 nanoseconds to +15 nanoseconds. The magnitude of the pulse at the upper and lower bounds of this time interval is a factor of 500 or more below the peak value of the pulse. Plots of the pulse shapes obtained after convolving the source pulse with TPART-III transmission data are shown in Figures 23 through 28. In Figures 23 and 26 the observed pulses for different receiver elevations peak at approximately zero retarded time. That is, there is essentially no time delay in the pulses observed for the different receiver elevations. The magnitude of the pulse does decrease, however, as the receiver elevation increases. The pulses for the zero receiver elevation were not plotted because the magnitude of those pulses were so much larger than the pulses for the other receiver elevations. Note that the pulses for the 14.7 source-receiver optical separation distance do not decrease at later times as rapidly as do those for the 5.3 source-receiver optical separation distance. This is a delayed response due to multiple scattering. The multiple scattering at the later times is not of sufficient magnitude to cause a shift in the peak of the pulse nor does multiple

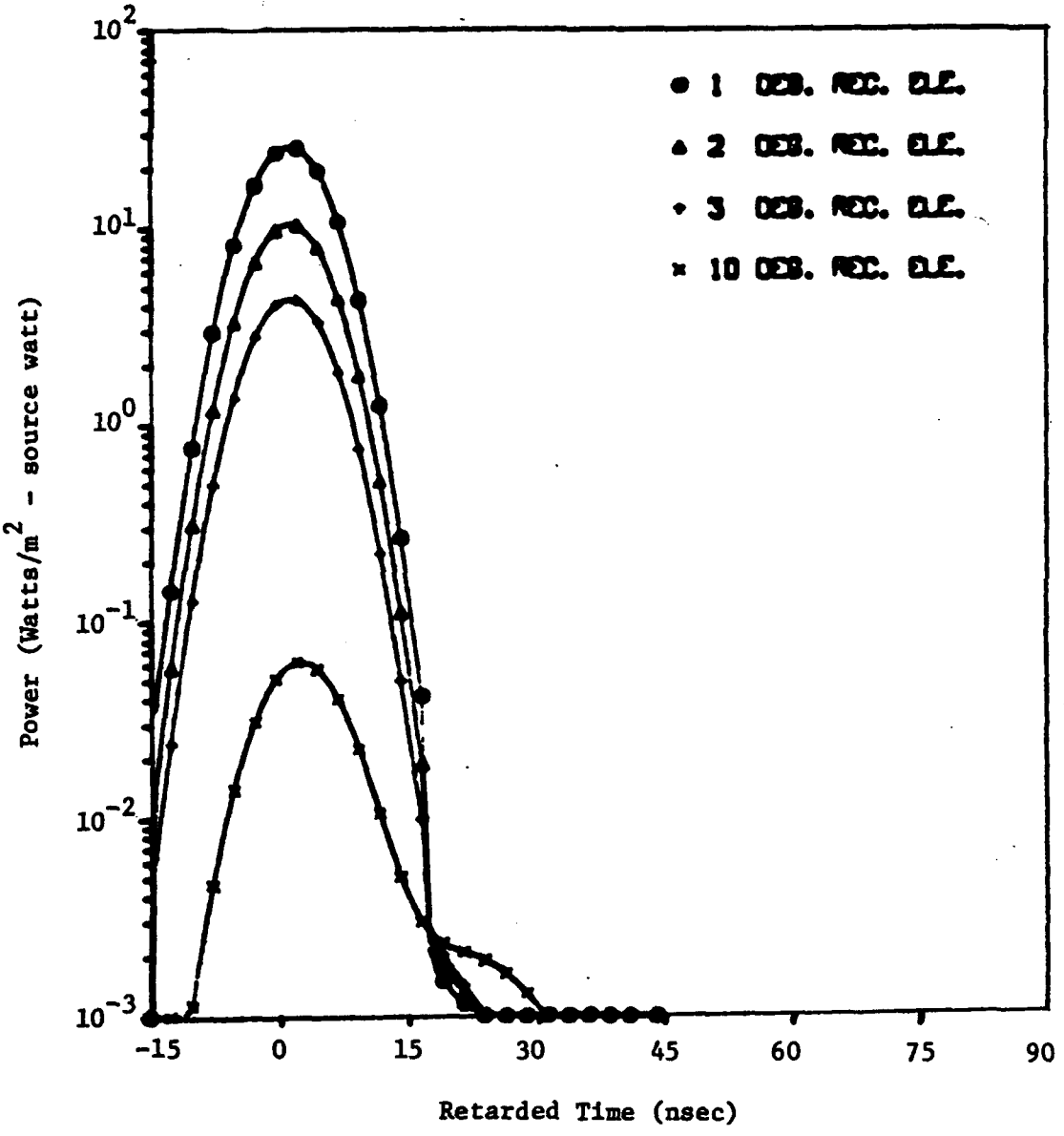

Fig. 23. Time Distribution of Scattered Laser Pulses Computed for a 0° Source Elevation and a 5.3 Source-Receiver Optical Separation Distance.

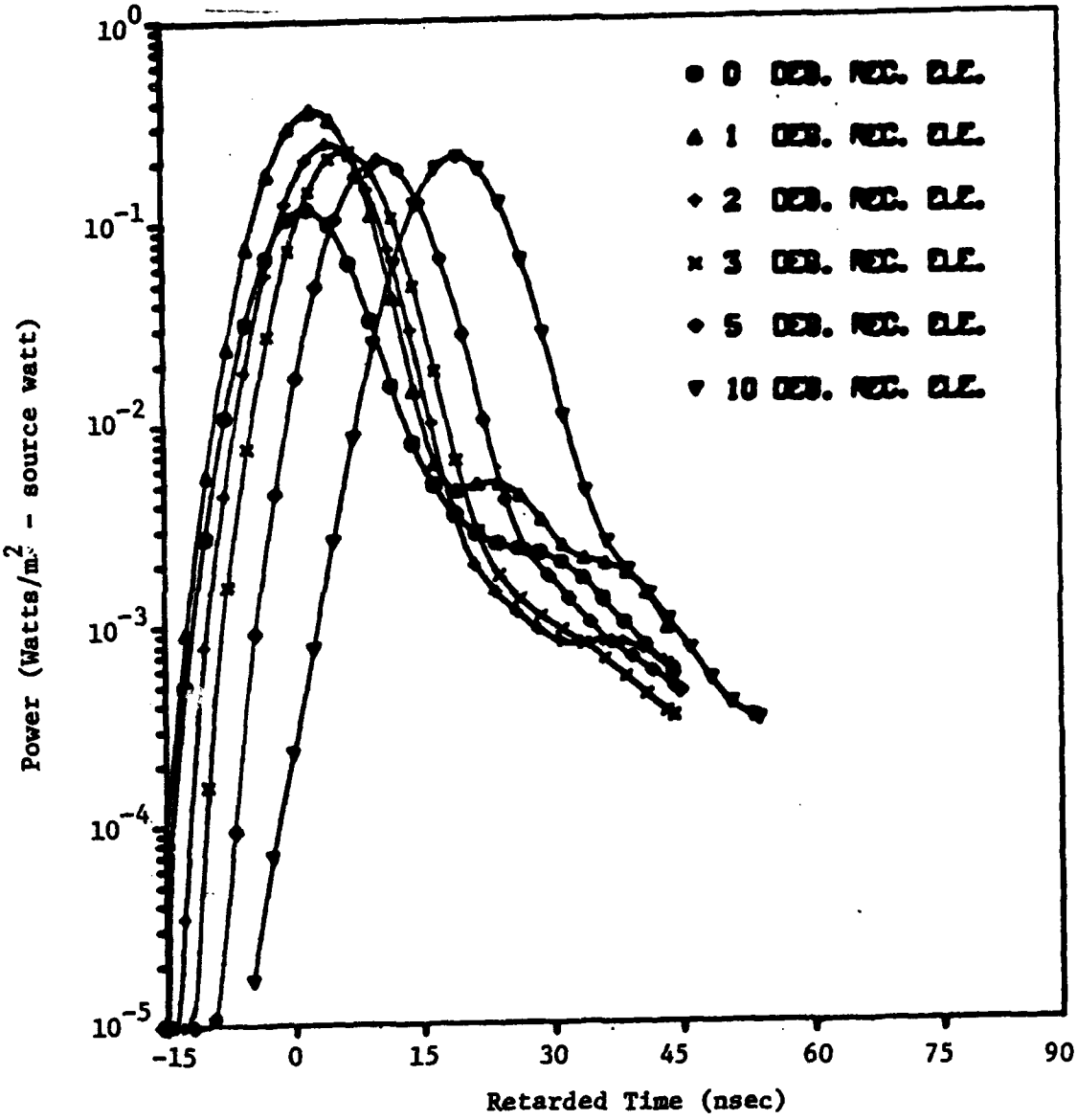

Fig. 24. Time Distribution of Scattered Laser Pulses Computed for a 5^o Source Elevation and a 5.3 Source-Receiver Optical Separation Distance.

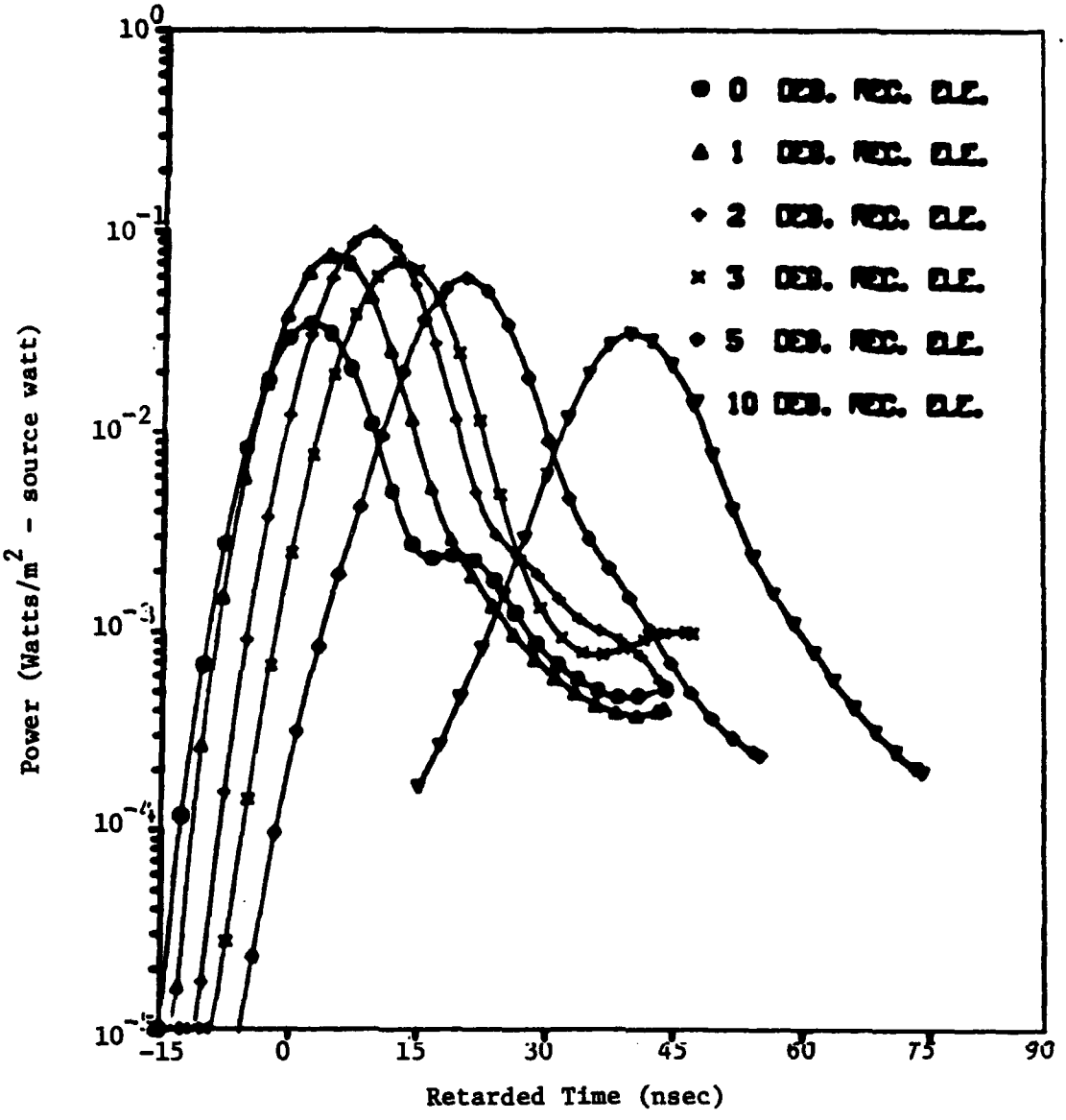

Fig. 25. Time Distribution of Scattered Laser Pulses Computed for a 10° Source Elevation and a 5.3 Source-Receiver Optical Separation Distance.

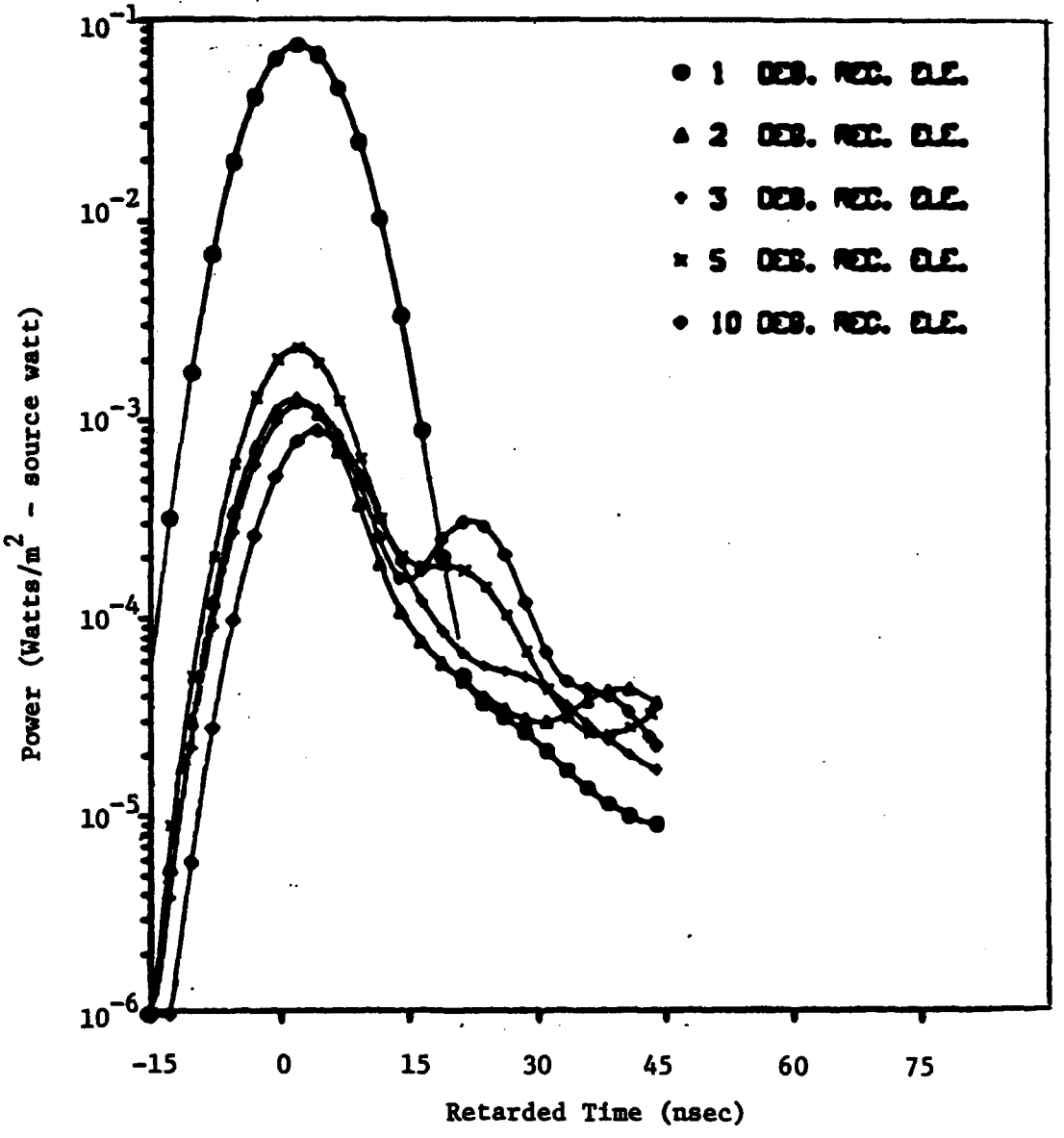

Fig. 26. Time Distribution of Scattered Laser Pulses Computed for a 0^{o} Source Elevation and a 14.7 Source-Receiver Optical Separation Distance.

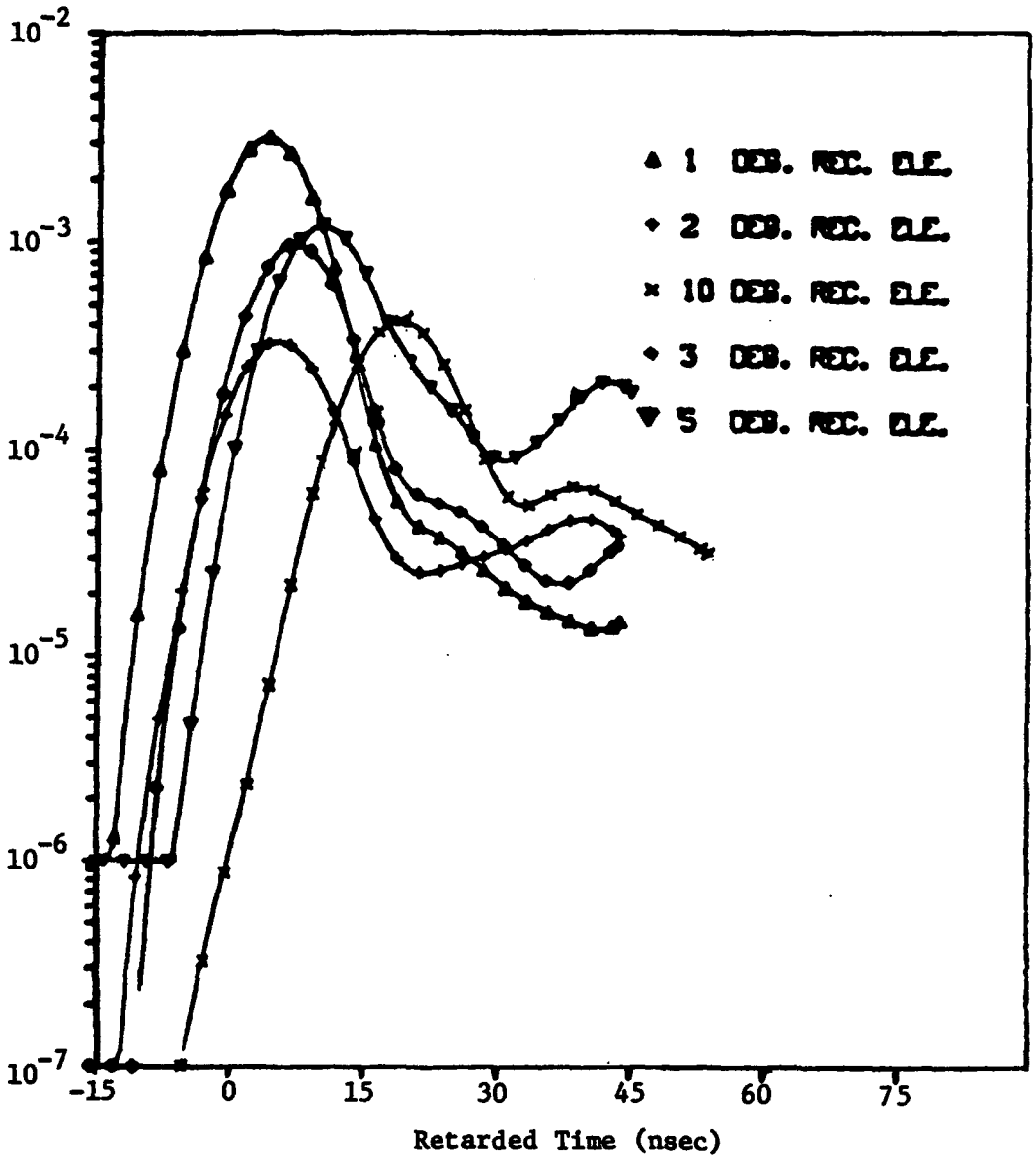

Fig. 27. Time Distribution of Scattered Laser Pulses Computed for a 5° Source Elevation and a 14.7 Source-Receiver Optical Separation Distance.

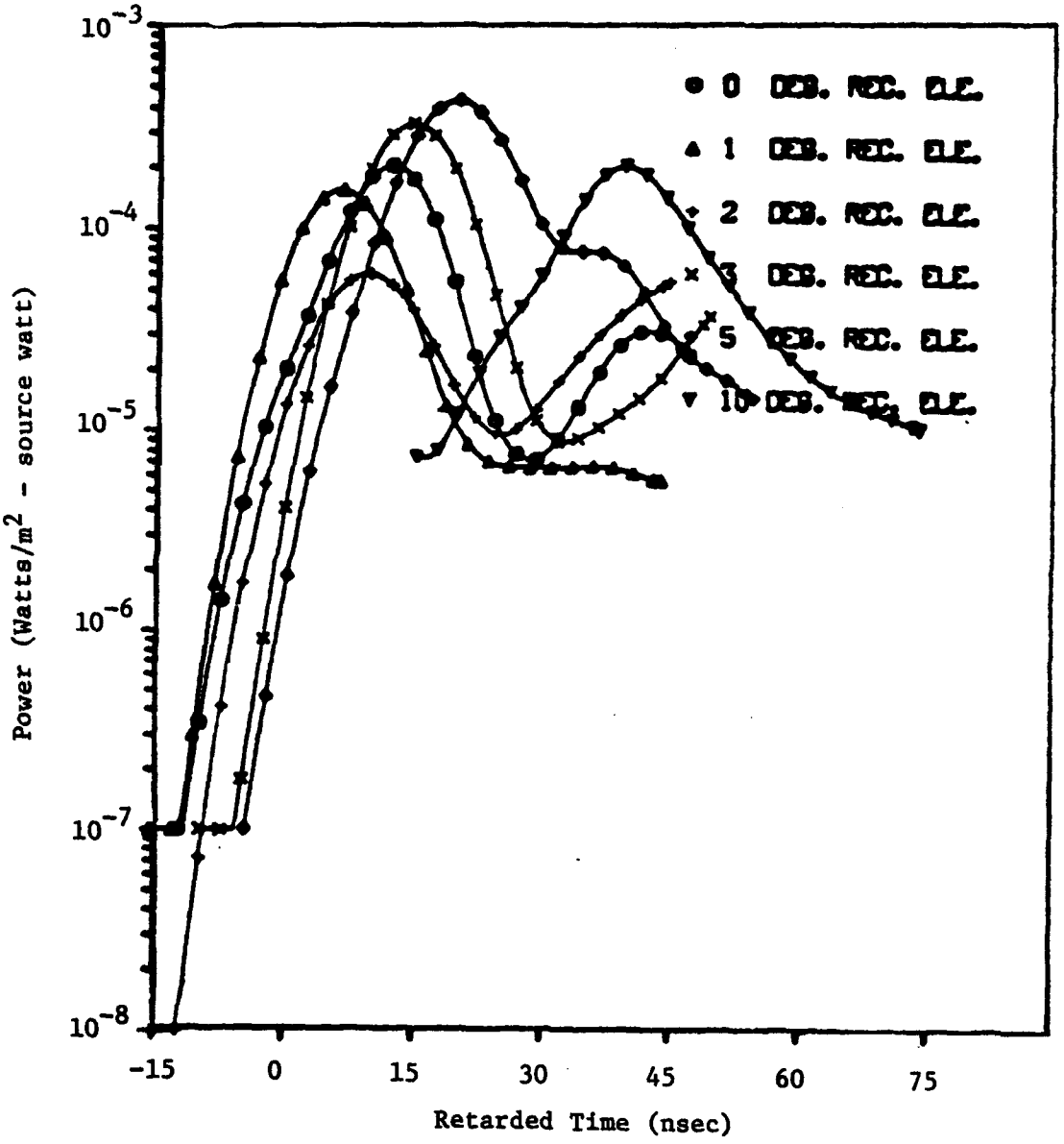

Fig. 28. Time Distribution of Scattered Laser Pulses Computed for a 10^{o} Source Elevation and a 14.7 Source-Receiver Optical Separation Distance.

scattering cause much broadening at the half-maximum point. (Note the pulse widths listed in Table IV.) In Figs. 24 and 27 the pulses computed for a source elevation of 5 degrees are plotted. The peaks in these pulses are shifted in time with the peak in the curve for a given receiver elevation occuring at approximately the time that the single-scattering response is expected to occur. Again it is noted that multiple scattering for the 14.7 source-receiver optical separation distance has more of an effect on the pulses at later times than it does for the 5.3 source-receiver optical separation distance.

The pulses computed for the 10-degree source elevation in Figs. 25 and 28 show results similar to that observed for the 5-degree source elevation. That is, the peaks in the curves shift to later times as the receiver is elevated to higher angles and multiple scattering has more of an effect in broadening the pulses for the 14.7 source-receiver optical separation distance than it does for the 5.3 source-receiver optical separation distance.

CONCLUSIONS

For the source-receiver arrangement and the cloud models considered in this study, a maximum time delay of approximately 40 nanoseconds was determined when both the source and receiver were scanned 10 degrees off the source-receiver axis. The time delays of the pulses computed for the various sources and receiver elevations corresponded to the time delay of the single-scattered radiation. This was true even though the major portion of the radiation received during the time periods of peak intensity was due to multiple scattering and not to single scattering. The time delays and pulse stretching value computed for the 5.3 and 14.7 source-receiver optical separation distances were similar. However, it appears that for the 14.7 source-receiver optical separation distance a smaller amount of the total scattered radiation was received during the time of peak intensity and that the time periods required to obtain 90 to 99 percent of the total scattered intensity were much longer than for the 5.3 source-receiver optical separation distance.

Pulse stretching, determined by comparing the widths of the pulses at half-maximum to the original half-maximum widths of the emitted pulse, was no more than 4 nanoseconds. However, the widths of the pulses at 0.1 maximum and lower appear to have been stretched considerably more than a few nanoseconds. This was especially true for the pulses computed for the 14.7 source-receiver optical separation distance.

The results of this study indicate that for the highly forward peaked phase functions, such as those determined for the clouds in Hawaii, the multiple-scattered light maintains its direction along the original laser beam for several orders of scattering. This phenomenon produces an effect similar to single scattering within a media with lower extinction coefficient.

REFERENCES

1. Collins, D. G., Transmission of Laser Light Within Foggy Atmospheres, Radiation Research Associates, Inc. Technical Report RRA-T7812 (December 1978)

2. Collins, D. G. and Wells, M. B., Effects of Atmospheric Scattering on Laser and Sunlight Transmissions in the Atmosphere, Radiation Research Associates, Inc. Technical Report RRA-T7707 (October 1977)

3. Blattner, W. G. M., Collins, D. G., and Wells, M. B., Computer Procedure for Calculating Light Scattering from Lasers, Radiation Research Associates, Inc. Technical Report RRA-T7708 (15 October 1977)

4. Earing, D. A. and Smith, I. A., Target Signatures Analysis Center: Data Compilation, Infrared and Optical Sensor Laboratory, Willow Run Laboratories, Institute of Science and Technology, The University of Michigan, Ann Arbor, Michigan (July 1966)

5. Blattner, W., Utilization Instructions for Operation of the MIE-2 Program on the Sandia CDC-6600 Computer, Radiation Research Associates, Inc. Technical Report RRA-T7707 (October 1977)